Fourier transformation microwave spectroscopy of the methyl glycolate-H2O complex

Fourier transformation microwave spectroscopy of the methyl glycolate–H_2O complex

Masaharu Fujitake, Toshihiro Tanaka and Nobukimi Ohashi

Division of Mathematical and Physical Sciences, Graduate School of Natural Science & Technology

Kanazawa University,

Kakuma-machi, Kanazawa, Ishikawa 920-1192, Japan.

Corresponding author : Masaharu Fujitake

Division of Mathematical and Physical Sciences, Graduate School of Natural Science & Technology, Kanazawa University

Kakuma-machi, Kanazawa, Ishikawa 920-1192, Japan

Tel : +81-76-264-5659

Fax : +81-76-264-5739

E-mail : fujitake@staff.kanazawa-u.ac.jp

***Abstract*:**

The rotational spectrum of one conformer of the methyl glycolate–H_2O complex has been measured by means of the pulsed jet Fourier transform microwave spectrometer. The observed *a*- and *b*-type transitions exhibit doublet splittings due to the internal rotation of the methyl group. On the other hand, most of the *c*-type transitions exhibit quartet splittings arising from the methyl internal rotation and the inversion motion between two equivalent conformations. The spectrum was analyzed using parameterized expressions of the Hamiltonian matrix elements derived by applying the tunneling matrix formalism. Based on the results obtained from ab initio calculation, the observed complex of methyl glycolate–H_2O was assigned to the most stable conformer of the insertion complex, in which a non-planer seven membered-ring structure is formed by the intermolecular hydrogen bonds between methyl glycolate and H_2O subunits. The inversion motion observed in the *c*-type transitions is therefore a kind of ring-inversion motion between two equivalent conformations. Conformational flexibility, which corresponds to the ring-inversion between two equivalent conformations and to the isomerization between two possible conformers of the insertion complex, was investigated with the help of the ab initio calculation.

***Keywords*:**

Methyl glycolate–H_2O complex

Rotational spectroscopy

Methyl internal rotation

Ring-inversion

Conformational flexibility

Funding: This research did not receive any specific grant from funding agencies in the public, commercial, or not-for-profit sectors.

1. Introduction

A number of hydrogen-bonded complexes between hydrophilic molecules and water have been studied extensively, because they might serve to understand various phenomena in liquids at the molecular level. Molecules having the intramolecular hydrogen bond are generally expected to form addition and insertion complexes with the water molecules. In the case of the addition complex, the water molecule forms a hydrogen bond to one of the available sites of the target molecule as a simple H-donor or H-acceptor, without breaking the existing intramolecular hydrogen bond. In the generation process of the insertion complex, a disruption of the intramolecular hydrogen bond and a construction of the intermolecular hydrogen bond network caused by the H_2O insertion need to occur simultaneously. Usually, the insertion complexes are more stable in energy compared to the addition complexes. However the molecular structure or the properties of the inserted molecule may change considerably from that of the monomer.

Methyl glycolate (MG), $CH_3O–C(=O)–CH_2–OH$, is a member of the α-hydroxyeste's family, and possesses both a hydrogen bond donor group (OH) and an acceptor groups (C=O / COC / COH) to form intramolecular hydrogen bond. MG has three different internal rotation axes (CC–OH, OC–C(=O) and (O=)C–OC) that can give rise to conformational isomers in addition to the methyl group internal rotation ($O–CH_3$). The interconversions between the conformers are allowed by the internal rotations hindered by relatively low potential barrier heights. The most stable conformer of MG is the *Ss* form in which the three CCOH, OCC=O and O=COC dihedral angles are close to 0° and being stabilized into the five-membered ring arrangement by an intramolecular OH⋯O=C hydrogen bond [1]. The intramolecular hydrogen bond makes the O–H stretching vibrational frequency significantly lower than that in the related aliphatic alcohols and also makes the CC–OH torsional frequency higher [2]. This conformer has three low-frequency torsional modes. The microwave spectra of this conformer in the vibrational ground state [3] and the torsionally excited states [4] have already been investigated. Analysis of the A–E methyl internal rotation splittings

observed in the microwave spectra yielded different effective V_3 barriers to the methyl internal rotation for the vibrational ground state and the torsionally excited states [3, 4]. Meyer et al. [5] analyzed combined data from microwave and far-infrared spectroscopy by a flexible model accounting for the methyl and two skeletal torsional modes. They suggested that the C–C torsion induces a change in the electronic structure of the carboxyl group to influence the methyl torsion through the intramolecular hydrogen bond. Six different conformers of MG were predicted by ab initio calculation and the two most stable conformers of MG were observed and characterized by vibrational spectroscopy [6].

Meanwhile, another α-hydroxyester, methyl lactate (ML) was investigated recently by free jet millimeter-wave absorption and molecular beam Fourier-transform microwave spectroscopy [7, 8]. The analysis of the spectrum was made to determine the rotational constants and the barrier height V_3 to the internal rotation of the CH_3–O methyl group in the vibrational ground state for the most stable conformer *SsC*. The *SsC* conformer forms the same five-membered ring structure as MG *Ss* due to the intramolecular hydrogen bond and also has similar torsional flexibility. Thomas et al. reported the rotational spectroscopic and ab initio theoretical studies on two kinds of the hydrogen bond clusters of ML, ML–NH_3 [9] and ML– $(H_2O)_{1,2}$ [10]. For both kinds of cluster, only the insertion type complexes, in which the ring structures are formed by the intermolecular hydrogen bonds, were identified. In the case of ML–NH_3, the NH_3 internal rotation was observed as well as the CH_3–O internal rotation, although the NH_3 subunit forms a OH···NH···O=C intermolecular hydrogen bond with ML. The internal rotation barrier height of the CH_3–O methyl group was found to be close to that of the ML monomer. In the case of ML–H_2O, the authors determined its conformation completely from four candidates with similar structure by combining the extensive isotopic studies. The wagging motion of the free H atom of H_2O subunit in ML–H_2O was investigated based on ab initio calculation, and the conversion barrier corresponding to the isomerization between the two most stable conformers was estimated to be low. The methyl

internal rotation barrier height of ML increases considerably upon hydration.

In this study, we report the rotational spectrum of a MG–H_2O complex by means of pulsed jet Fourier transform microwave spectroscopy. The MG–H_2O complex is expected to form the hydrogen bond network of the seven membered ring in the most stable insertion type conformation as well as the ML–H_2O complex. However, because of the high symmetry of MG, the MG–H_2O complex has a feasible large amplitude motion between two equivalent mirror images belonging to the same conformer, in addition to the methyl internal rotation. Parameterized expressions of the Hamiltonian matrix elements suitable for the analysis of the rotational spectrum of MG–H_2O were derived by applying the tunneling matrix formalism developed by Hougen [11]. The tunneling matrix formalism is extremely useful for the analysis of the molecular spectrum in which tunneling splittings caused by more than two kinds of the large amplitude vibrational motions appear. The conformational structure of the observed conformer was assigned by comparing the spectroscopic constants determined experimentally with those obtained by ab initio calculation. Conformational flexibility, which gives rise to the large amplitude motion between two equivalent conformations and to the isomerization between two possible conformers of the insertion complex of MG–H_2O, was investigated with the help of ab initio calculation.

2. Experimental

Rotational spectra of the MG monomer and the MG–H_2O complex were observed in the 8 – 26 GHz region by means of the pulsed supersonic jet Fourier-transform microwave (FTMW) spectrometer which has been described elsewhere [12]. A commercial sample of MG (Sigma-Aldrich) was used without further purification. The liquid sample of MG was put into a reservoir nozzle and maintained the temperature around 50 °C by electrical heating in order to increase the concentration of MG in the supersonic jet. Pure neon gas (Takachiho Trading Co., Ltd.) was used as a carrier gas at a stagnation pressure of about 800 kPa. For the observation of

MG–H_2O complexes, the neon carrier gas was seeded with water vapor by passing through a liquid water reservoir which was inserted between the inlet of the nozzle and the carrier gas line, and kept at room temperature. The MG / Ne or MG / H_2O / Ne mixture was then injected into a vacuum chamber by a pulsed solenoid valve (~ 0.8 mm orifice diameter) at a repetition rate of ~ 2 Hz to create supersonic beam. The molecules in the beam were polarized with 0.5 – 2.0 μs microwave pulses and subsequent free-induction decay (FID) time-domain signal from the molecules was digitized for 4096 or 8192 points at an 8 MHz clock rate. Depending on the signal intensity, 300 – 20,000 FID signals were averaged in order to get a sufficient signal-to-noise ratio. The averaged FID data were then Fourier transformed to obtain the frequency-domain power spectrum. Since the supersonic jet beam axis and the Fabry–Pérot resonator axis were arranged coaxially, each transition was observed as a doublet due to the Doppler-effect. The transition frequency was thus determined by averaging the peak frequencies of the two Doppler components. The estimated accuracy of the frequency measured is better than 2 kHz for the unblended lines.

3. Theoretical calculation ---- ab-initio quantum chemistry calculation

We carried out ab initio calculations on the MG monomer and the MG–H_2O complexes to predict the molecular properties relevant to the interpretation of the rotational spectra of the possible conformers, such as rotational constants, electric dipole moments and methyl internal rotation parameters as well as relative energies and harmonic vibrational frequencies. All calculations were performed using the Gaussian 09W program package [13].

For the MG monomer, only the most dominant conformer (*Ss*) was optimized at the MP2/aug-cc-pVTZ level of theory and the spectroscopic parameters were estimated.

The six most stable conformers of MG–H_2O optimized at the MP2/aug-cc-pVTZ level of theory are shown in Fig. 1, and the energies and spectroscopic properties for each conformer are given in Table 1. The label of each atom in MG and H_2O distinguished by a number is shown in

Fig. 1, where the hydrogen groups {H(10), H(11), H(12)} and {H(5), H(8)} correspond to the methyl group and the methylene group of MG, respectively. For H_2O, a hydrogen bonding H atom is labeled as H(14) and another H atom which is free from the hydrogen bonding is H(15). These conformers were derived from the most dominant conformation of MG monomer (*Ss*). Two conformers named as "In- a" and "In-b" are the insertion complexes, and "a" and "b" classify the direction of the hydrogen-bond free H(15) atom of H_2O. Remaining conformers, "Ad(Z)" or "Ad(Z)-X" (Z = OH, O=C, COC and X = CH_2 or Me), are the addition complexes where "Z" specifies the oxygen atom of the hydration site in MG which accepts a proton of H_2O to form the intermolecular hydrogen bond. In the case of Ad(COC), the orientation of H_2O is also distinguished by the index X. The In-a conformer is the most stable one and is similar to the "i-I" conformer of methyl lactate–H_2O complex reported by Thomas et al. [10]. Optimized structural parameters for the two most stable conformers, In-a and In-b, of MG–H_2O are available as Supplementary material (Table S1 in the Supplementary material).

For the insertion type conformers of MG–H_2O, counterpoise corrections [14, 15] were also computed, but this correction yield no significant changes to the relative energy and the optimized structure.

Especially in the case of the insertion type complex, hydration distorts the structure of the MG subunit significantly from the equilibrium structure of the MG monomer. We calculated the energy of the virtual MG monomer having the same structure in the complex and then subtracted the energy of MG monomer in equilibrium structure from the energy of virtual MG to obtain the deformation energy caused by the hydration. Similarly, the deformation energy of H_2O subunit was also estimated. Calculated deformation energies, $E_{\mathrm{def}}(\mathrm{MG})$, $E_{\mathrm{def}}(\mathrm{H_2O})$, and $E_{\mathrm{def}}(\mathrm{total}) \equiv E_{\mathrm{def}}(\mathrm{MG}) + E_{\mathrm{def}}(\mathrm{H_2O})$ are given in Table 1.

Table 1

Energies (relative energy and deformation energy), rotational constants, dipole moment μ_g and methyl group internal rotation parameters (inertial moment I_α and direction cosines λ_g) of six most stable conformers of MG–H_2O calculated at MP2/aug-cc-pvtz level of theory (g = a, b, c).

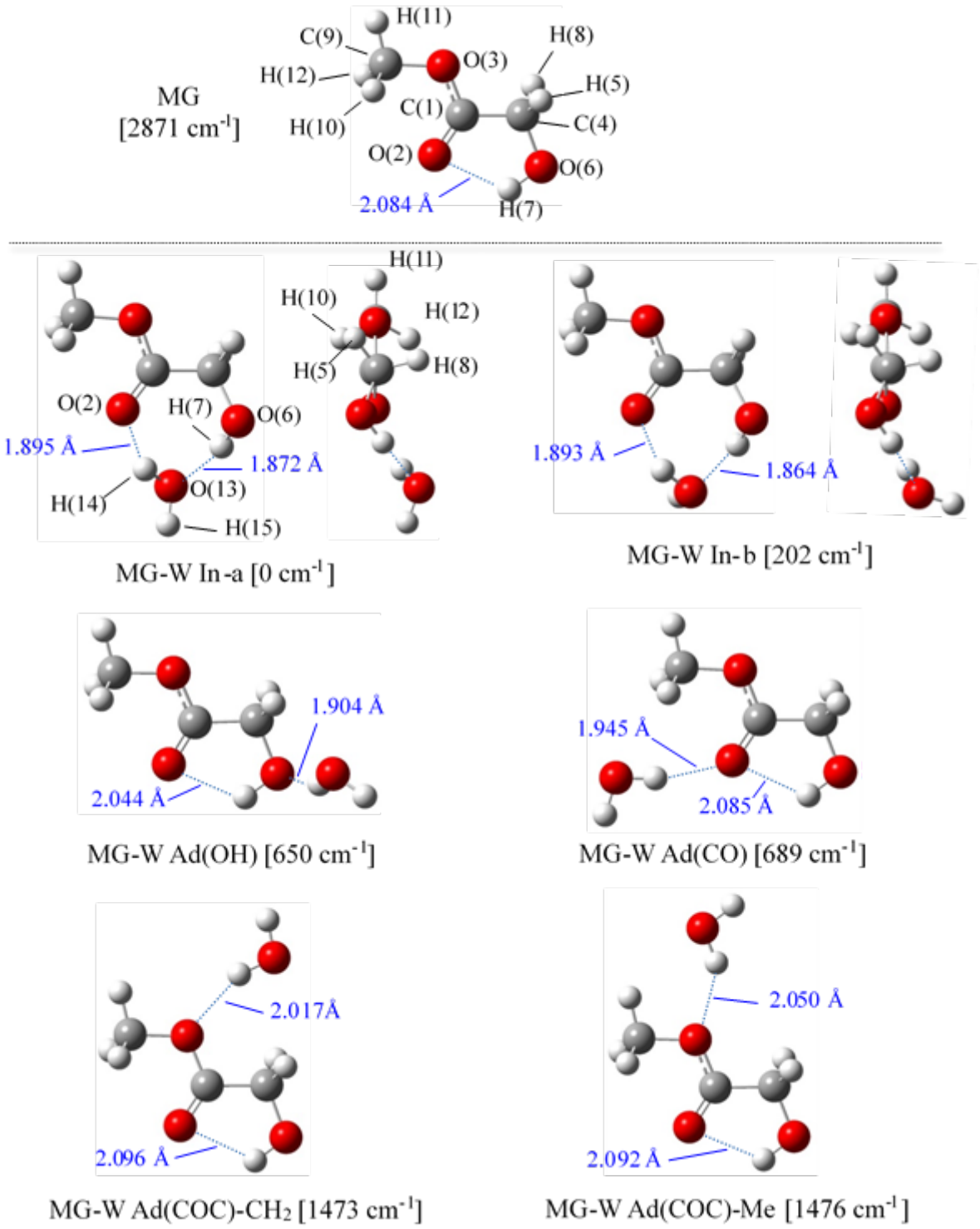

Fig. 1. Optimized geometries of the MG monomer and the six most stable conformers of the MG–H_2O complex calculated at the MP2/aug-cc-pVTZ level of theory. The relative energies and the hydrogen bond length are also given for the MG–H_2O complexes.

	In-a	In-b	Ad(OH)	Ad(CO)	Ad(COC) -CH_2	Ad(COC) -OMe
ΔE_e [a]/ cm^{-1}	0	202	650	689	1473	1476
ΔE_{e+ZPE} [b] / cm^{-1}	0	179	457	449	1068	1075
E_{def}(MG)[c] / cm^{-1}	742	764	31	37	37	15
E_{def} (H_2O)[c] / cm^{-1}	41	44	23	14	8	8
E_{def}(total)[c] / cm^{-1}	783	807	54	51	44	23
A_e / MHz	4042	4074	4777	3637	2390	3825
B_e / MHz	1469	1455	1094	1382	1947	1263
C_e / MHz	1136	1121	1018	1014	1088	961
κ[d]	-0.771	-0.774	-0.960	-0.719	0.320	-0.789
$\lvert \mu_a \rvert$ / D	2.36	3.22	1.98	0.07	3.57	1.54
$\lvert \mu_b \rvert$ / D	1.00	1.09	0.05	1.45	2.88	0.85
$\lvert \mu_c \rvert$ / D	0.25	2.57	0.98	0.00	0.01	0.00
$\lvert \mu \rvert$ / D	2.57	4.26	2.21	1.45	4.59	1.76
I_α / uÅ^2	3.2055	3.2053	3.2072	3.2044	3.2065	3.2174
$\lvert \lambda_a \rvert$	0.670	0.664	0.883	0.994	0.222	0.502
$\lvert \lambda_b \rvert$	0.733	0.739	0.013	0.112	0.975	0.865
$\lvert \lambda_c \rvert$	0.118	0.115	0.470	0.000	0.001	0.000

[a] Relative electronic energy and the absolute value for the In-a conformer is - 419.394498 E_h.

[b] Relative energy including zero-point vibrational energy under harmonic approximation and the absolute value for the In-a conformer is - 419.273174 E_h.

[c] Deformation energy caused by the structural change from the equilibrium structure of monomer after complex formation (see text).

[d] Ray's asymmetry parameter defined by (2*B*-*A*-*C*)/(*A*-*C*).

The structure having *Cs*-symmetry, which is expected to be a transition state of a large amplitude motion between two equivalent forms of the In-a conformer, was also optimized with restricting the symmetry. In addition, two kinds of isomerization potential curve between the In-a and In-b conformers were computed by performing a relaxed potential energy surface scan along the internal coordinates defined by the dihedral angles of *D*(1-4-6-7) and *D*(15-13-14-2). The dihedral

angle dependences of the rotational constants, the deformation energy, and Wiberg bond index [16] were also estimated for the two isomerization process. We did not succeed in the calculation of the potential energy surface corresponding to the two-dimensional scan along *D*(1-4-6-7) and *D*(15-13-14-2) by relaxed potential energy surface scan carried out at the MP2/aug-cc-pVTZ level of theory.

4. Tunneling–rotational Hamiltonian matrix elements and Determination of V_3

4.1. Parameterized expression of the Hamiltonian matrix elements

Theoretical formalism used in this study is essentially equivalent to that described in Ref.12, where parameterized expressions of the Hamiltonian matrix elements were derived for the analysis of the rotational spectrum of N-methylaniline in the ground vibrational state by applying the tunneling matrix formalism developed by Hougen [11]. We revised the formalism to adjust to the analysis of the MG-H_2O complex.

(1) Permutation-inversion group for the MG-H_2O complex

We assume that a large amplitude motion between two equivalent forms of the MG-H_2O complex interrelated by a mirror plane is feasible as well as the internal rotation of a methyl group. In the case of the insertion type conformers, the former motion can be regarded as a ring-inversion because they have a non-planar seven-membered intermolecular ring structure containing two intermolecular hydrogen bonds. The three H atoms of the methyl group of MG are specified by numbers 10, 11, and 12, and two H atoms of the methylene group are 5 and 8 (see Fig. 1). The permutation-inversion (PI) group of MG-H_2O is therefore G_6, which has six operations: $O_1 \equiv E$, $O_2 \equiv (10\ 11\ 12)$, $O_3 \equiv (10\ 12\ 11)$, $O_4 \equiv (10\ 12)(5\ 8)^*$, $O_5 \equiv (10\ 11)(5\ 8)^*$, and $O_6 \equiv (11\ 12)(5\ 8)^*$. The O_2 and O_3 operations denote CH_3 internal rotation and O_4, O_5, and O_6 correspond to the

ring-inversion. This PI group has three irreducible representations A_1, A_2, and E and the character table is given in Table 2 together with the nuclear spin statistical weight.

Table 2
Character table of the permutation-inversion group G_6 and nuclear statistical weight for MG-H_2O.

	O_1 = E	O_2 = (10 11 12) O_3 = (10 12 11)	O_4 = (10 12)(5 8)* O_5 = (10 11)(5 8)* O_6 = (11 12)(5 8)*	nuclear statistical spin weight
A_1	1	1	1	32
A_2	1	1	-1	32
E	2	-1	0	32

Three H atoms of the methyl group of MG are specified by numbers 10, 11, and 12, and two H atoms of the methylene group are 5 and 8 (see Fig. 1).

(2) Vibrational framework functions

There are in principle six frameworks corresponding to the six feasible PI operations. We denote each vibrational framework function localized in the potential minimum by

$$\left| i : local \right\rangle = \mathrm{O}_i \left| 1 : local \right\rangle \qquad (n = 1, 2, 3, 4, 5 \text{ and } 6)\,, \tag{1}$$

where, the framework of n = 1 corresponds to the atomic specification shown in Fig. 1 and 6. Then six new vibrational framework functions $\left| n \right\rangle (n = 1, 2, \cdots, 6)$ which are orthogonal to each other are introduced by using the following relations [17, 18]:

$$\left| n \right\rangle = \sum_{i=1}^{6} (\mathbf{\Delta}^{-1/2})_{n,i} \left| i : local \right\rangle \quad (n = 1, 2, 3, \cdots, 6)\,, \tag{2}$$

$$\langle n \mid m \rangle = \delta_{n,m} \qquad (m,n = 1,2,\cdots,6), \tag{3}$$

where $\mathbf{\Delta}^{-1/2} \equiv \mathbf{S}\,\mathbf{d}^{-1/2}\,\mathbf{S}^{\dagger}$, and $\mathbf{d} \equiv \mathbf{S}^{\dagger}\,\mathbf{\Delta}\,\mathbf{S}$ is a diagonal matrix consisting of positive eigenvalues obtained by applying a unitary transformation **S** to **Δ**. **Δ** is a matrix composed of overlap integrals

$$(\Delta)_{n,m} \equiv \langle n : local \mid m : local \rangle \; (m,n = 1,2,\cdots,6). \tag{4}$$

The new framework functions also satisfy the relation [17]:

$$\mid n \rangle = \mathrm{O}_n \mid 1 \rangle \ . \tag{5}$$

Using these vibrational frame functions $\mid n \rangle$, we produced symmetrized vibrational functions

$$\mid \mathrm{A}_1 \rangle_{vib} + \mid \mathrm{A}_2 \rangle_{vib} + 2 \mid \mathrm{E} \rangle_{vib} . \tag{6}$$

For the nondegenerate –symmetry species, we define the following symmetrized functions:

$$\begin{aligned} \mid \mathrm{A}_1 \rangle &= \frac{1}{\sqrt{6}} \left[\mid 1 \rangle + \mid 2 \rangle + \mid 3 \rangle + \mid 4 \rangle + \mid 5 \rangle + \mid 6 \rangle \right], \\ \mid \mathrm{A}_2 \rangle &= \frac{1}{\sqrt{6}} \left[\mid 1 \rangle + \mid 2 \rangle + \mid 3 \rangle - \mid 4 \rangle - \mid 5 \rangle - \mid 6 \rangle \right]. \end{aligned} \tag{7}$$

Hereafter, we exclude the subscript *vib* for convenience. The transformation properties of the symmetrized vibrational functions of A species under the PI group operations are

$$\begin{aligned} &(10\ 11\ 12) \mid \mathrm{A}_1 \rangle = \mid \mathrm{A}_1 \rangle, \qquad (10\ 12)(5\ 8)^* \mid \mathrm{A}_1 \rangle = \mid \mathrm{A}_1 \rangle \\ &(10\ 11\ 12) \mid \mathrm{A}_2 \rangle = \mid \mathrm{A}_2 \rangle, \qquad (10\ 12)(5\ 8)^* \mid \mathrm{A}_2 \rangle = - \mid \mathrm{A}_2 \rangle, \ \textit{etc.} \end{aligned} \tag{8}$$

On the other hand, two sets of the symmetrized functions belonging to the nondegenerate E species exist. We denote them by $\left(\mid \mathrm{E}(1)_a \rangle, \mid \mathrm{E}(1)_b \rangle \right)$ and $\left(\mid \mathrm{E}(2)_a \rangle, \mid \mathrm{E}(2)_b \rangle \right)$, and adopt the following functions:

$$
\begin{aligned}
|\,\mathrm{E}(1)_a\,\rangle &= \frac{1}{\sqrt{6}}\left[|\,1\,\rangle + \omega^2|\,2\,\rangle + \omega|\,3\,\rangle + |\,4\,\rangle + \omega|\,5\,\rangle + \omega^2|\,6\,\rangle\right],\\
|\,\mathrm{E}(1)_b\,\rangle &= \frac{1}{\sqrt{6}}\left[|\,1\,\rangle + \omega|\,2\,\rangle + \omega^2|\,3\,\rangle + |\,4\,\rangle + \omega^2|\,5\,\rangle + \omega|\,6\,\rangle\right],\\
|\,\mathrm{E}(2)_a\,\rangle &= \frac{1}{\sqrt{6}}\left[|\,1\,\rangle + \omega^2|\,2\,\rangle + \omega|\,3\,\rangle - |\,4\,\rangle - \omega|\,5\,\rangle - \omega^2|\,6\,\rangle\right],\\
|\,\mathrm{E}(2)_b\,\rangle &= \frac{1}{\sqrt{6}}\left[|\,1\,\rangle + \omega|\,2\,\rangle + \omega^2|\,3\,\rangle - |\,4\,\rangle - \omega^2|\,5\,\rangle - \omega|\,6\,\rangle\right],
\end{aligned}
\tag{9}
$$

where $\omega = \exp(i\,2\pi/3)$. The transformation properties of these symmetrized vibrational functions of E species under the PI group operations are

$$
\begin{aligned}
&(10\ 11\ 12)|\,\mathrm{E}(1)_a\,\rangle = \omega|\,\mathrm{E}(1)_a\,\rangle,\ (10\ 11\ 12)|\,\mathrm{E}(1)_b\,\rangle = \omega^2|\,\mathrm{E}(1)_b\,\rangle,\\
&(10\ 12)(5\ 8)^*|\,\mathrm{E}(1)_a\,\rangle = |\,\mathrm{E}(1)_b\,\rangle,\\
&(10\ 11\ 12)|\,\mathrm{E}(2)_a\,\rangle = \omega|\,\mathrm{E}(2)_a\,\rangle,\ (10\ 11\ 12)|\,\mathrm{E}(2)_b\,\rangle = \omega^2|\,\mathrm{E}(2)_b\,\rangle,\\
&(10\ 12)(5\ 8)^*|\,\mathrm{E}(2)_a\,\rangle = -|\,\mathrm{E}(2)_b\,\rangle,\quad \textit{etc.}
\end{aligned}
\tag{10}
$$

(3) Transformation properties of Eulerian angles, total angular momentum operators and rotational functions under the generating operations of G_6

By taking a tunneling path model and a coordinate system in an appropriate way, for the ring-inversion - internal rotation - overall rotation problem, we have such a molecule-fixed reference axis system that the axes coincide with the principal axes in the equilibrium configuration, and in the coordinate system Eulerian angles χ, θ, and ϕ are transformed under the generating operations (10 11 12) and (10 12)(5 8)* of the PI group G_6 as:

$$
\begin{aligned}
&(10\ 11\ 12)[\chi,\theta,\phi] = [\chi,\theta,\phi],\\
&(10\ 12)(5\ 8)^*[\chi,\theta,\phi] = [\pi-\chi,\pi-\theta,\pi+\phi].
\end{aligned}
\tag{11}
$$

The transformation properties of the total angular momentum operators are

$$
\begin{aligned}
&(10\ 11\ 12)\begin{bmatrix} J_X \\ J_Y \\ J_Z \end{bmatrix} = \begin{bmatrix} J_X \\ J_Y \\ J_Z \end{bmatrix}, \quad (10\ 12)(5\ 8)^* \begin{bmatrix} J_X \\ J_Y \\ J_Z \end{bmatrix} = \begin{bmatrix} J_X \\ J_Y \\ J_Z \end{bmatrix}, \\
&\begin{bmatrix} J_x \\ J_y \\ J_z \end{bmatrix} = S(\chi,\theta,\phi)\begin{bmatrix} J_X \\ J_Y \\ J_Z \end{bmatrix}, \quad (10\ 11\ 12)\begin{bmatrix} J_x \\ J_y \\ J_z \end{bmatrix} = \begin{bmatrix} J_x \\ J_y \\ J_z \end{bmatrix}, \quad (10\ 12)(5\ 8)^* \begin{bmatrix} J_x \\ J_y \\ J_z \end{bmatrix} = \begin{bmatrix} -J_x \\ J_y \\ -J_z \end{bmatrix},
\end{aligned}
\tag{12}
$$

and those of the symmetric-top wave functions are

$$
\begin{aligned}
&(10\ 11\ 12)\left| J,K \right\rangle = \left| J,K \right\rangle \\
&(10\ 12)(5\ 8)^* \left| J,K \right\rangle = (-1)^{J-K} \left| J,-K \right\rangle.
\end{aligned}
\tag{13}
$$

(4) Phenomenological Hamiltonian operator

In the present study, we employed the following phenomenological Hamiltonian operator including centrifugal distortion corrections of Watson's A-reduced type [19],

$$
\begin{aligned}
H = {} & h_{\mathrm{v}} + AJ_z^{\ 2} + BJ_x^{\ 2} + C_y^{\ 2} \\
& - \Delta_J \mathbf{J}^4 - \Delta_{JK}\mathbf{J}^2 J_z^{\ 2} - \Delta_K J_z^{\ 4} - 2\delta_J \mathbf{J}^2\left(J_x^{\ 2} - J_y^{\ 2}\right) - \delta_K\left[J_z^{\ 2}\left(J_x^{\ 2} - J_y^{\ 2}\right) + \left(J_x^{\ 2} - J_y^{\ 2}\right)J_z^{\ 2}\right] \\
& + i\left(q_z + q_{zJ}\mathbf{J}^2 + q_{zK}J_z^{\ 2}\right)J_z + iq_x J_x + iq_y J_y .
\end{aligned}
\tag{14}
$$

All coefficients appeared in the Hamiltonian operator (h_{v}, A, B, C, Δ_J, $\cdots$, q_z, $\cdots$) are the functions of the large amplitude motion variables. Each coefficient has the following transformation properties under operations:

$$
\begin{aligned}
&(10\ 11\ 12)T = T, \quad (10\ 12)(5\ 8)^* T = T, \quad T^* = T, \quad T^{\ddagger} = T \quad \text{for } T = h_{\mathrm{v}}, A, B, C, \Delta_J, \Delta_{JK},, \Delta_K, \delta_J, \delta_K \\
&(10\ 11\ 12)R = R, \quad (10\ 12)(5\ 8)^* R = -R, \quad R^* = R, \quad R^{\ddagger} = -R \quad \text{for } R = q_z, q_{zJ}, q_{zK}, \text{and } q_x \\
&(10\ 11\ 12)q_y = q_y, \quad (10\ 12)(5\ 8)^*(12)^* q_y = q_y, \quad q_y^* = q_y, \quad q_y^{\ddagger} = -q_y
\end{aligned}
\tag{15}
$$

where ‡ denotes the combined operation of time-reversal and Hermitian conjugation.

(5) Parameterized expression of the Hamiltonian matrix elements

We denote the vibration-rotation basis function by

$$\left| J,K;\Gamma \right\rangle \equiv \left| J,K \right\rangle \left| \Gamma \right\rangle, \quad \left(\Gamma = \mathrm{A}_1,\ \mathrm{A}_2, \mathrm{E}(1)_a, \mathrm{E}(1)_b, \mathrm{E}(2)_a, \text{and } \mathrm{E}(2)_b \right), \tag{16}$$

where Γ specifies not the symmetry of the vibration-rotation function but the symmetry of the symmetrized vibrational functions.

Parameterized expression of the Hamiltonian matrix elements in the vibration-rotation basis $\left| J,K;\Gamma \right\rangle$ can be derived by utilizing the transformation properties mentioned above. However, in this study, we took only four tunneling $\left| 1 \right\rangle \to \left| n \right\rangle$ $(n = 1,2,3,4)$ into consideration and ignored $\left| 1 \right\rangle \to \left| 5 \right\rangle$ and $\left| 1 \right\rangle \to \left| 6 \right\rangle$ tunneling. Both of $\left| 1 \right\rangle \to \left| 5 \right\rangle$ and $\left| 1 \right\rangle \to \left| 6 \right\rangle$ tunneling are the combination motions of the methyl internal rotation and the ring-inversion. Furthermore, the *J*- and *K*-dependence of $\left| 1 \right\rangle \to \left| 4 \right\rangle$ (ring-inversion) was also ignored.

Under this approximation, the Hamiltonian matrix elements for the A-species are

$$\begin{aligned}
&\left\langle J,K;\mathrm{A}_\zeta \left| H \right| J,K';\mathrm{A}_\zeta \right\rangle \\
&= \sum_{n=1}^{2} f_n \Big[\left\langle 1 \left| h_\mathrm{v} \right| n \right\rangle \delta_{K,K'} + \left\langle 1 \left| A \right| n \right\rangle K^2 \delta_{K,K'} \\
&\qquad + \left\langle 1 \left| B \right| n \right\rangle \left\langle J,K \left| J_x^{\,2} \right| J,K' \right\rangle + \left\langle 1 \left| C \right| n \right\rangle \left\langle J,K \left| J_y^{\,2} \right| J,K' \right\rangle \\
&\qquad - \left\langle 1 \left| \Delta_J \right| n \right\rangle J^2 (J+1)^2 \delta_{K,K'} - \left\langle 1 \left| \Delta_{JK} \right| n \right\rangle J(J+1) K^2 \delta_{K,K'} - \left\langle 1 \left| \Delta_K \right| n \right\rangle K^4 \delta_{K,K'} \\
&\qquad\qquad - 2 \left\langle 1 \left| \delta_J \right| n \right\rangle J(J+1) \left\langle J,K \left| J_x^{\,2} - J_y^{\,2} \right| J,K' \right\rangle \\
&\qquad\qquad\qquad - \left\langle 1 \left| \delta_K \right| n \right\rangle \left\langle J,K \left| J_z^{\,2} \left(J_x^{\,2} - J_y^{\,2} \right) + \left(J_x^{\,2} - J_y^{\,2} \right) J_z^{\,2} \right| J,K' \right\rangle \Big] \\
&\quad - (-1)^\zeta \left\langle 1 \left| h_\mathrm{v} \right| 4 \right\rangle \delta_{K,K'},
\end{aligned} \tag{17}$$

and

$$\left\langle J,K;\mathrm{A}_1 \left| H \right| J,K';\mathrm{A}_2 \right\rangle = \left\langle J,K;\mathrm{A}_2 \left| H \right| J,K';\mathrm{A}_1 \right\rangle = 0, \tag{18}$$

where ζ = 1 and 2, and f_1 = 1 and f_2 = 2. Therefore, $\left\langle J,K;\mathrm{A}_1 \left| H \right| J,K';\mathrm{A}_1 \right\rangle$ block and $\left\langle J,K;\mathrm{A}_2 \left| H \right| J,K';\mathrm{A}_2 \right\rangle$ block give the vibration-rotation energy levels corresponding to the A_1

and A_2 species of the vibrational symmetry, respectively. The rotational energy level structures of the A_1 and A_2 species are equivalent except for the energy shift by $\pm\langle 1 \mid h_{\mathrm{v}} \mid 4 \rangle$.

For the degenerate-symmetry E species,

$$\begin{aligned}
&\langle J,K;\mathrm{E}(1)_{\mathrm{a}} \,|H|\, J,K';\mathrm{E}(1)_{\mathrm{b}} \rangle = 0,\\
&\langle J,K;\mathrm{E}(2)_{\mathrm{a}} \,|H|\, J,K';\mathrm{E}(2)_{\mathrm{b}} \rangle = 0,\\
&\langle J,K;\mathrm{E}(1)_{\mathrm{a}} \,|H|\, J,K';\mathrm{E}(2)_{\mathrm{b}} \rangle = 0,
\end{aligned} \tag{19}$$

and, consequently, the Hamiltonian matrix of the E species is divided into two independent submatrices of a- and b-component blocks. Since these two submatrices give the equivalent set of the eigenvalues and eigenfunctions, we treated the following type of the Hamiltonian (sub)matrix without distinguishing the a- and b-components for the E species.

$$\left[\begin{array}{c:c}
\langle J,K;\mathrm{E}(1) \,|H|\, J,K';\mathrm{E}(1) \rangle & \langle J,K;\mathrm{E}(1) \,|H|\, J,K';\mathrm{E}(2) \rangle \\
\hdashline
\langle J,K;\mathrm{E}(2) \,|H|\, J,K';\mathrm{E}(1) \rangle & \langle J,K;\mathrm{E}(2) \,|H|\, J,K';\mathrm{E}(2) \rangle
\end{array}\right] \tag{20}$$

This Hamiltonian matrix consists of four blocks and the matrix elements are given by

$$\begin{aligned}
&\langle J,K;\mathrm{E}(\zeta) \,|H|\, J,K';\mathrm{E}(\zeta) \rangle\\
&= \sum_{n=1}^{2} g_n \Big[\langle 1 \,|h_{\mathrm{v}}|\, n \rangle \delta_{K,K'} + \langle 1 \,|A|\, n \rangle K^2 \delta_{K,K'}\\
&\qquad + \langle 1 \,|B|\, n \rangle \langle J,K \,|J_x^{\,2}|\, J,K' \rangle + \langle 1 \,|C|\, n \rangle \langle J,K \,|J_y^{\,2}|\, J,K' \rangle\\
&\qquad - \langle 1 \,|\Delta_J|\, n \rangle J^2 (J+1)^2 \delta_{K,K'} - \langle 1 \,|\Delta_{JK}|\, n \rangle J(J+1) K^2 \delta_{K,K'} - \langle 1 \,|\Delta_K|\, n \rangle K^4 \delta_{K,K'}\\
&\qquad\qquad - 2\langle 1 \,|\delta_J|\, n \rangle J(J+1) \langle J,K \,|J_x^{\,2} - J_y^{\,2}|\, J,K' \rangle\\
&\qquad\qquad\qquad - \langle 1 \,|\delta_K|\, n \rangle \langle J,K \,|J_z^{\,2}(J_x^{\,2} - J_y^{\,2}) + (J_x^{\,2} - J_y^{\,2}) J_z^{\,2}|\, J,K' \rangle \Big]\\
&\quad - (-1)^{\zeta} \langle 1 \,|h_{\mathrm{v}}|\, 4 \rangle \delta_{K,K'} + \sqrt{3} \langle 1 \,|q_z|\, 2 \rangle K \delta_{K,K'} + \sqrt{3} \langle 1 \,|q_x|\, 2 \rangle \langle J,K \,|J_x|\, J,K' \rangle,
\end{aligned} \tag{21}$$

$$\begin{aligned}\langle J,K;\mathrm{E}(1)\,|H|\,J,K';\mathrm{E}(2)\rangle &= \sqrt{3}\langle 1\,|q_y|\,2\rangle\langle J,K\,|J_y|\,J,K'\rangle,\\ \langle J,K;\mathrm{E}(2)\,|H|\,J,K';\mathrm{E}(1)\rangle &= \sqrt{3}\langle 1\,|q_y|\,2\rangle\langle J,K\,|J_y|\,J,K'\rangle,\end{aligned} \tag{22}$$

where $\zeta = 1$ and 2, and $g_1 = 1$ and $g_2 = -1$.

For the analysis of the MG monomer, we employed the Hamiltonian matrix elements which can be obtained from the $\langle J,K;\mathrm{A}_1\,|H|\,J,K';\mathrm{A}_1\rangle$ block of Eq. (17) and the $\langle J,K;\mathrm{E}(1)\,|H|\,J,K';\mathrm{E}(1)\rangle$ block of Eq. (21) by simply eliminating the ring-inversion $\langle 1\,|\,h_\mathrm{v}\,|\,4\rangle$ term. Those are basically the same as the matrix elements used in the previous study of N-methylaniline [12].

4.2. Selection Rule for the Rotational Transitions of MG–H_2O.

By taking into consideration the transformation properties of the dipole moment operator $\boldsymbol{\mu}$ in the molecular-fixed reference axis (z, x, y) under the PI group operations

$$(10\ 11\ 12)\begin{bmatrix}\mu_x\\ \mu_y\\ \mu_z\end{bmatrix}=\begin{bmatrix}\mu_x\\ \mu_y\\ \mu_z\end{bmatrix},\qquad (10\ 12)(5\ 8)^*\begin{bmatrix}\mu_x\\ \mu_y\\ \mu_z\end{bmatrix}=\begin{bmatrix}\mu_x\\ -\mu_y\\ \mu_z\end{bmatrix},\ \ etc., \tag{23}$$

we obtained the following dipole moment matrix elements with respect to the symmetrized vibrational functions of A species when neither component of the permanent dipole is zero;

$$\begin{aligned}&\langle \mathrm{A}_1\,|\mu_z|\,\mathrm{A}_1\rangle \neq 0, \quad \langle \mathrm{A}_2\,|\mu_z|\,\mathrm{A}_2\rangle \neq 0, \quad \langle \mathrm{A}_1\,|\mu_z|\,\mathrm{A}_2\rangle = 0,\\ &\langle \mathrm{A}_1\,|\mu_x|\,\mathrm{A}_1\rangle \neq 0, \quad \langle \mathrm{A}_2\,|\mu_x|\,\mathrm{A}_2\rangle \neq 0, \quad \langle \mathrm{A}_1\,|\mu_x|\,\mathrm{A}_2\rangle = 0,\\ &\langle \mathrm{A}_1\,|\mu_y|\,\mathrm{A}_1\rangle = 0, \quad \langle \mathrm{A}_2\,|\mu_y|\,\mathrm{A}_2\rangle = 0, \quad \langle \mathrm{A}_1\,|\mu_y|\,\mathrm{A}_2\rangle \neq 0.\end{aligned} \tag{24}$$

Therefore, selection rules for the vibrational symmetries of A species are

$\mathrm{A}_1 \leftrightarrow \mathrm{A}_1$ and $\mathrm{A}_2 \leftrightarrow \mathrm{A}_2$ for the "z-type" and "x-type" rotational transition,

and

$\mathrm{A}_1 \leftrightarrow \mathrm{A}_2$ for the "y-type" rotational transition.

On the other hand, the symmetry consideration for the E-species leads to

$$\langle E(i)|\mu_\alpha|E(j)\rangle \neq 0 \quad (i, j = 1,2;\ \alpha = x, y, z)\,. \tag{25}$$

When $\langle 1|\mu_\alpha|1\rangle \neq 0$ and $\langle n|\mu_\alpha|n'\rangle = \langle 1|\mu_\alpha|1\rangle\delta_{n,n'}$ ($\alpha = z, x, y$ and $n, n' = 1, 2, 3, 4, 5, 6$) are assumed, the dipole moment matrix elements can be approximated by

$$\begin{aligned}
&\langle \mathrm{A}_1|\mu_z|\mathrm{A}_1\rangle \approx \langle 1|\mu_z|1\rangle, && \langle \mathrm{A}_2|\mu_z|\mathrm{A}_2\rangle \approx \langle 1|\mu_z|1\rangle, && \langle \mathrm{A}_1|\mu_z|\mathrm{A}_2\rangle = 0,\\
&\langle \mathrm{A}_1|\mu_x|\mathrm{A}_1\rangle \approx \langle 1|\mu_x|1\rangle, && \langle \mathrm{A}_2|\mu_x|\mathrm{A}_2\rangle \approx \langle 1|\mu_x|1\rangle, && \langle \mathrm{A}_1|\mu_x|\mathrm{A}_2\rangle = 0,\\
&\langle \mathrm{A}_1|\mu_y|\mathrm{A}_1\rangle = 0, && \langle \mathrm{A}_2|\mu_y|\mathrm{A}_2\rangle = 0, && \langle \mathrm{A}_1|\mu_y|\mathrm{A}_2\rangle \approx \langle 1|\mu_y|1\rangle,
\end{aligned} \tag{26}$$

and

$$\begin{aligned}
&\langle \mathrm{E}(1)|\mu_z|\mathrm{E}(1)\rangle \approx \langle 1|\mu_z|1\rangle, && \langle \mathrm{E}(2)|\mu_z|\mathrm{E}(2)\rangle \approx \langle 1|\mu_z|1\rangle, && \langle \mathrm{E}(1)|\mu_z|\mathrm{E}(2)\rangle \approx 0,\\
&\langle \mathrm{E}(1)|\mu_x|\mathrm{E}(1)\rangle \approx \langle 1|\mu_z|1\rangle, && \langle \mathrm{E}(2)|\mu_x|\mathrm{E}(2)\rangle \approx \langle 1|\mu_z|1\rangle, && \langle \mathrm{E}(1)|\mu_x|\mathrm{E}(2)\rangle \approx 0,\\
&\langle \mathrm{E}(1)|\mu_y|\mathrm{E}(1)\rangle \approx 0, && \langle \mathrm{E}(2)|\mu_y|\mathrm{E}(2)\rangle \approx 0, && \langle \mathrm{E}(1)|\mu_y|\mathrm{E}(2)\rangle \approx \langle 1|\mu_y|1\rangle.
\end{aligned} \tag{27}$$

Eq. (25) suggests that every combination of the vibrational symmetries of E species, E(1) and E(2), is allowed for the rotational transition in principle. But two intrastate components (E(1) – E(1) and E(2) – E(2)) are dominant in the "*z*-type" and "*x*-type" rotational transition and the interstate components (E(1) – E(2) and E(1) – E(2)) are dominant in the "*y*-type" rotational transition under this approximation.

Since it is expected that the *z*, *x*, *y* axes system is nearly equivalent to the principal axes system of inertia for MG-H_2O we describe hereafter "*z*-type", "*x*-type", and "*y*-type" transition as *a*-type, *b*-type, and *c*-type transition, respectively, for convenience.

4.3. Determination of the barrier height to internal rotation of the methyl group V_3

In this study, the barrier height to internal rotation of the methyl group V_3 and the direction cosine for the internal rotation axis were determined from observed values of the Coriolis-coupling-like tunneling parameters $\langle 1 | q_g | 2 \rangle$ and the rotational parameters $\langle 1 | B_g | 2 \rangle$,

where $g = z, x, y$ and B_z, B_x and B_y denote A, B and C. If the methyl group internal rotation and the ring-inversion are assumed to be motions independent of each other, the following useful relations can be derived by comparing Eqs. (17), (21), and (22) with the traditional effective Hamiltonian matrix for the one methyl top internal rotation derived under a simple high-barrier approximation [20, 21, 22],

$$\sqrt{3}\langle 1 | q_g | 2 \rangle = -2F\lambda_g \frac{I_\alpha}{I_g} \langle 0, \mathrm{E} | p | 0, \mathrm{E} \rangle \quad (g = z, x, y), \tag{28}$$

$$3\langle 1 | B_g | 2 \rangle = 4F^2 \rho_g^2 \left\{ \sum_{\mathrm{v}' \neq 0} \frac{\left| \langle 0, \mathrm{A} | p | \mathrm{v}', \mathrm{A} \rangle \right|^2}{E_0^{(\mathrm{A})} - E_{\mathrm{v}'}^{(\mathrm{A})}} - \sum_{\mathrm{v}' \neq 0} \frac{\left| \langle 0, \mathrm{E} | p | \mathrm{v}', \mathrm{E} \rangle \right|^2}{E_0^{(\mathrm{E})} - E_{\mathrm{v}'}^{(\mathrm{E})}} \right\} \quad (g = z, x, y), \tag{29}$$

where λ_g ($g = z, x, y$ and $\lambda_z^2 + \lambda_z^2 + \lambda_z^2 = 1$) is a g-component of the direction cosine, and I_α is the moment of inertia of the methyl top about its symmetry axis. I_g's are the inertial moments of the entire molecule and are estimated from $\langle 1 | B_g | 1 \rangle$ using following equation,

$$I_g = \frac{h}{8\pi^2 \langle 1 | B_g | 1 \rangle} \quad (g = z, x, y). \tag{30}$$

F is the reduced rotational constant for internal rotation defined by

$$F = \frac{\hbar^2}{2rI_\alpha}, \quad r = 1 - \sum_g \lambda_g \rho_g, \quad \rho_g = \lambda_g \frac{I_\alpha}{I_g}. \tag{31}$$

The angular momentum operator of the methyl internal rotation is denoted by p. The torsional energies $E_{\mathrm{v}}^{(\Gamma)}$, the eigen functions $| \mathrm{v}, \Gamma \rangle$ and the matrix elements $\langle 0, \Gamma | p | \mathrm{v}', \Gamma \rangle$ were obtained by numerically solving the Schrodinger equation

$$\left[Fp^2 + \frac{1}{2} V_3 (1 - \cos 3\alpha) \right] | \mathrm{v}, \Gamma \rangle = E_{\mathrm{v}}^{(\Gamma)} | \mathrm{v}, \Gamma \rangle \quad (\Gamma = \mathrm{A} \text{ and } \mathrm{E}), \tag{32}$$

where α denotes the internal rotation angle.

5. Observed spectra and analysis

5.1. Methyl glycolate monomer

Before investigating MG–H_2O, we measured the rotational spectrum of MG in the ground vibrational state of the *Ss* conformer in the 11 – 17 GHz region and assigned 18 (13 *a*-type + 5 *b*-type) rotational transitions. Three of them ($4_{04} - 3_{03}$, $4_{14} - 3_{13}$, and $3_{12} - 2_{11}$) have already been reported in the previous study [5]. All rotational transitions observed in the present FTMW spectroscopy exhibit doublet structure (A and E components) due to the methyl internal rotation, and measured transition frequencies are all given in Table S2 (supplementary material). The measured frequencies were fitted using a least-squares procedure and spectroscopic parameters of MG thus determined are presented in Table 3 as well as internal rotation parameters. The barrier height V_3 and the direction cosine $|\lambda_z|$ of the internal rotation parameters were estimated mainly from $\langle 1 | q_z | 2 \rangle$, $\langle 1 | q_x | 2 \rangle$, $\langle 1 | A | 2 \rangle$, and $\langle 1 | B | 2 \rangle$ by using the theoretical value of I_α and $\lambda_y = 0$ ($\lambda_z^2 + \lambda_x^2 = 1$) assumption. Values of the rotational constants and the internal rotation parameters obtained with the principal axis method (PAM) by Caminati and Cervellati [3] are also given in Table 3 for comparison. It is shown that the results obtained in this study are in agreement with those reported in the previous study [3] and that they have been determined with a greater accuracy.

Table 3

Spectroscopic and internal rotation parameters[a] of MG in the ground state.

	This work	Ref.[3]
$\langle 1 \mid A \mid 1 \rangle$ / MHz	10001.3140(60)	10001.33(9)
$\langle 1 \mid B \mid 1 \rangle$ / MHz	2204.0018(10)	2204.082(6)
$\langle 1 \mid C \mid 1 \rangle$ / MHz	1849.28409(71)	1849.249(6)
$\langle 1 \mid \Delta_J \mid 1 \rangle$ / kHz	0.191(23)	
$\langle 1 \mid \Delta_{JK} \mid 1 \rangle$ / kHz	1.174(48)	
$\langle 1 \mid \delta_J \mid 1 \rangle$ / kHz	0.0287(44)	
$\langle 1 \mid A \mid 2 \rangle$ /MHz	0.9912(31)	
$\langle 1 \mid B \mid 2 \rangle$ /MHz	0.01011(14)	
$\langle 1 \mid C \mid 2 \rangle$ /MHz	-0.00118(17)	
$\langle 1 \mid q_z \mid 2 \rangle$ /MHz	16.567(51)	
$\langle 1 \mid q_{zJ} \mid 2 \rangle$ / kHz	-0.672(94)	
$\langle 1 \mid q_{zK} \mid 2 \rangle$ / kHz	-41(13)	
$\langle 1 \mid q_x \mid 2 \rangle$ / MHz	1.78(76)	
rms[b] / MHz	0.0016	
N[c]	36	
V_3 / cm^{-1}	394.5(10)	396(31)
I_α / uÅ^2	3.2056 [Fixed][d]	3.20[Fixed]
$\mid \lambda_z \mid$[e]	0.9059(61)	0.896(14)
$\mid \lambda_x \mid$[e]	0.423(13)	0.443(28)
F / GHz	166.76	166.9

[a] Values in parentheses denote 3 times standard deviation in units of the last digit.

[b] Root mean square deviation of the fit.

[c] Number of lines.

[d] Theoretical value obtained by ab initio calculation at MP2/aug-cc-pvtz.

[e] Absolute value of the direction cosine of the internal rotation axis to the molecular fixed z or x axis.

5.2. Methyl glycolate – H_2O complex: In-a conformer

The spectrum assignment of MG–H_2O complex was carried out by using the theoretically predicted spectrum as a preliminary guess. First, we simulated the rigid rotor spectrum of the most stable conformer In-a based on the theoretical values of the rotational constants (A = 4042, B = 1467, C = 1136 MHz and $\kappa = (2B - A - C)/(A - C) = -0.77$) and the values of three components of the electric dipole moment ($|\mu_a|$ = 2.36, $|\mu_b|$ = 1.00, $|\mu_c|$ = 0.25 D) given in Table 1. After that we decided to start with the search of three intense *a*-type *R*-branch transition series; $J+1_{0\,J+1} - J_{0\,J}$, $J+1_{1\,J+1} - J_{1\,J}$, and $J+1_{1\,J} - J_{1\,J-1}$. The assignment of such *a*-type *R*-branch transitions was executed smoothly. Subsequently, we proceeded to the assignment of the *a*-type *R*-branch transitions with higher K_a (≤ 4) or to the *b*-type *R*- and *Q*-branch transitions expected to be slightly weaker. All the *a*- and *b*-type transitions assigned in this study exhibit the doublet structures which can be analyzed as the methyl group internal rotation splittings. Examples of the doublet are shown in Fig. 2-(a) and 2-(b). The largest values of the splitting width observed in the *a*-type and *b*-type transitions are about 6.9 MHz and 20.5 MHz, respectively.

Then, we progressed to the measurement of the *c*-type transition which is predicted to be very weak compared with *a*- and *b*-type transitions. We began with the assignment of $J+1_{1\,J} - J_{0\,J}$ (J = 2 – 4) among the *c*-type transitions and found that they consist of weak quartet with comparable intensity as shown in Fig.2-(c). This quartet has a structure in which both A and E components of the internal rotation were further split into doublets with a narrow frequency gap of about 0.04 MHz. Finally, we assigned the *c*-type transitions with $K_a \leq 3$. All of the additional doublets belonging to the A-symmetry species of them have almost equal splitting width of ~ 0.039 MHz. Also, the E-species components usually have the doublet structure of the same splitting width as the A-species except for several transitions which indicate intensity anomaly described later. We attributed this additional splitting to the ring-inversion motion, which was theoretically treated in Section 4.1 by

applying the tunneling matrix formalism.

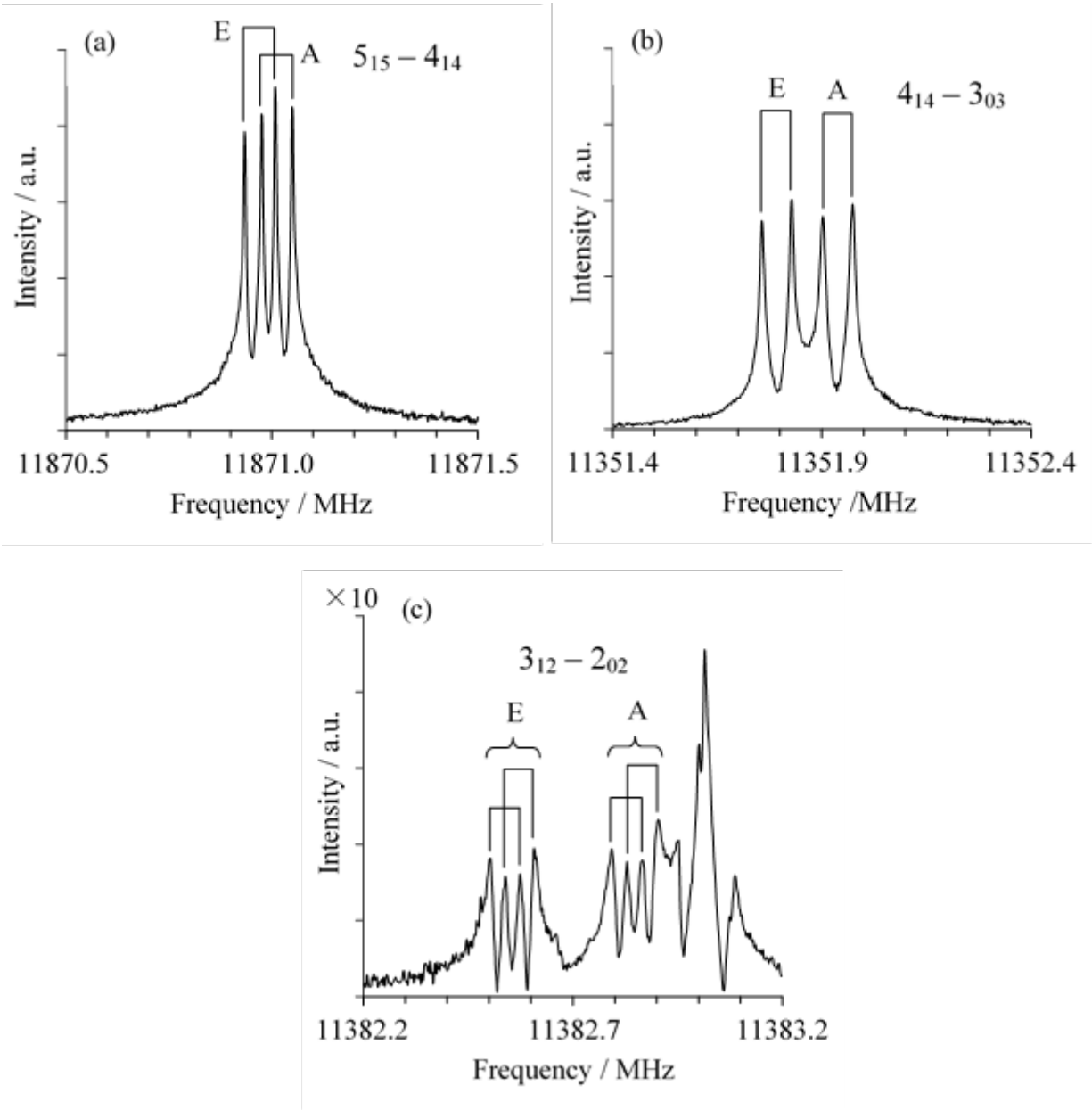

Fig. 2. Examples of the representative spectrum of MG–H_2O. (a) and (b) are the *a*- and *b*-type transitions, respectively, and exhibit the methyl group internal rotation doublet structure. (c) is the *c*-type transition which shows a quartet structure caused by the internal rotation and the ring-inversion motion.

Such features of the observed splittings can be interpreted basically by applying the selection rules described in Section 4.2 to the energy level structure, in which the E(1) and E(2) species of the

vibrational symmetry have the equivalent rotational energy level structure within the measurement accuracy except for the energy shift by $\pm\langle 1 | h_v | 4 \rangle$ as well as the case of the A_1 and A_2 species. Each component of the doublet observed in the *a*- and *b*-type transitions was thus assigned to the overlap line of $A_1 - A_1 + A_2 - A_2$, or E(1) – E(1) + E(2) – E(2) as shown in Fig. 2-(a) and –(b). On the other hand, two sets of the additional doublet which were observed in the *c*-type transitions are the pair of the $A_1 - A_2$ and $A_2 - A_1$ interstate components and the pair of the E(1) – E(2) and E(2) – E(1) components, as shown in Fig.2-(c). The splitting width of all additional doublets is constant and is expressed by $4\langle 1 | h_v | 4 \rangle$. The assignment of the interstate components of a given rotational transition was decided so that the energy of the A_2 / E(2) state become higher than the A_1 / E(1) state. All the transition frequencies of MG–H_2O observed in this study are given in Table S3 (Supplementary material).

As mentioned above, intensity anomalies were observed in several transitions of the E-species. Fig. 3 shows examples of the observed FTMW spectrum of MG–H_2O, in which the A – E splitting widths and the intensities are compared between the *b*- and *c*-type transition group of $(J, K_a) = (3, 3) - (2, 2)$. In the cases of the *b*-type transitions of $3_{3\,1} - 2_{2\,0}$ and $3_{3\,0} - 2_{2\,1}$, the E-symmetry component of the internal rotation doublet is very weak compared to that of the A component. In contrast, the E-symmetry species of the *c*-type transitions of $3_{3\,0} - 2_{2\,0}$ and $3_{3\,1} - 2_{2\,1}$ appear with considerably larger intensity than A, and furthermore, the intrastate E(1) – E(1) + E(2) – E(2) overlap line is observed instead of the interstate doublet of E(1) – E(2) and E(2) – E(1) although clearly resolved spectrum of $A_1 - A_2$ and $A_2 - A_1$ doublet is observed with weak intensity. By taking into consideration the symmetric-top nature of the rotational wave function corresponding to the $K_a \cong J$ level in the E-symmetry species [23], a qualitative explanation with respect to such behavior of the spectral intensity will be obtained.

On the other hand, symmetrical triplets were observed in the E-symmetry species of the *c*-type transitions of $2_{2\,1} - 1_{1\,1}$, $2_{2\,0} - 1_{1\,0}$, $5_{3\,3} - 4_{2\,3}$, and $5_{3\,2} - 4_{2\,2}$. The triplet consists of two

interstate components, E(1) – E(2) and E(2) – E(1), and one intrastate E(1) – E(1) + E(2) – E(2) overlap line, as shown in Fig. 4. The intrastate component appears exactly in the center frequency of the interstate doublet.

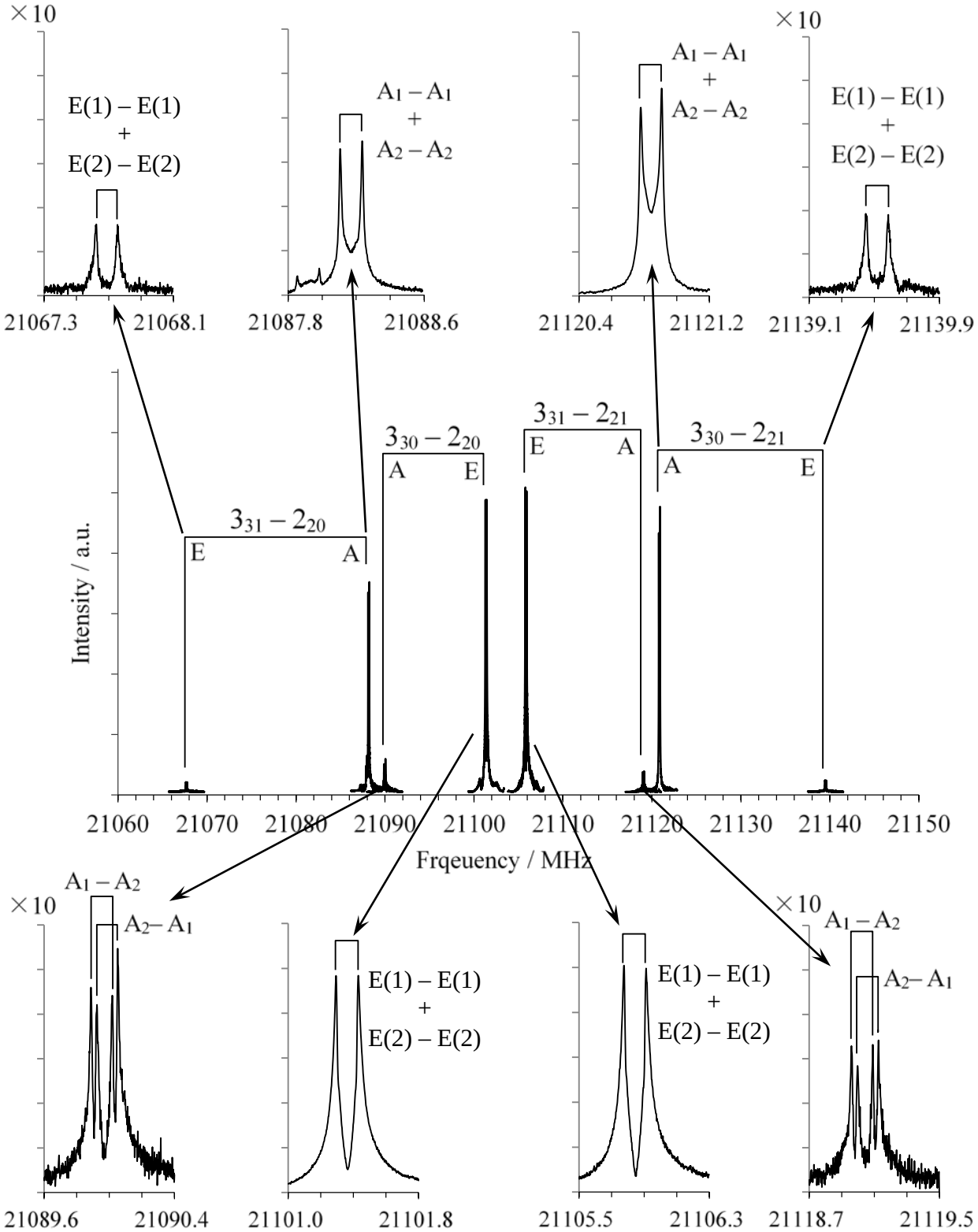

Fig. 3. Intensity anomalies observed in the *b*- and *c*-type transition group of (J, K_a) = (3, 3) – (2, 2) of MG–H_2O.

In order to solve completely the problem of the intensity anomalies mentioned above, it is necessary to build the formalism for the transition moment including the effects of both the methyl group internal rotation and the ring-inversion. However, we have not conducted the quantitative analysis of the spectral intensity here.

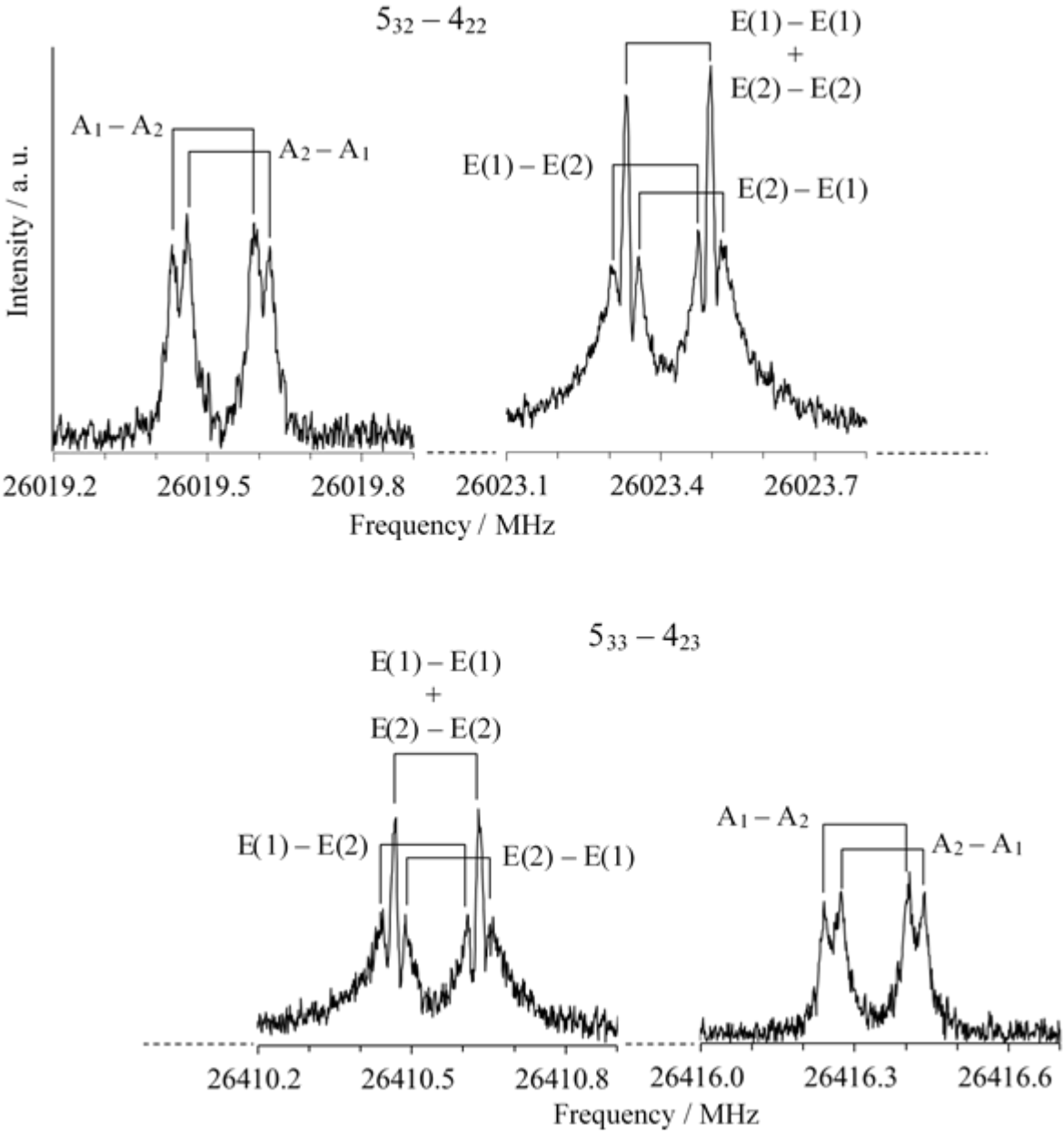

Fig. 4. Symmetrical triplets observed in the E-symmetry species of the *c*-type transitions, $5_{3\,3} - 4_{2\,3}$ and $5_{3\,2} - 4_{2\,2}$, of MG–H_2O.

Table 4

Spectroscopic and internal rotation parameters of MG – H_2O in the ground state [a].

$\langle 1 \mid A \mid 1 \rangle$ / MHz	3963.70764(30)	$\langle 1 \mid A \mid 2 \rangle$ / MHz	0.059438(56)
$\langle 1 \mid B \mid 1 \rangle$ / MHz	1448.41134(10)	$\langle 1 \mid B \mid 2 \rangle$ / MHz	0.008147(27)
$\langle 1 \mid C \mid 1 \rangle$ / MHz	1115.69161(8)	$\langle 1 \mid C \mid 2 \rangle$ / MHz	-0.000270(20)
$\langle 1 \mid \Delta_J \mid 1 \rangle$ / kHz	0.45700(88)	$\langle 1 \mid q_z \mid 2 \rangle$ / MHz	3.24537(79)
$\langle 1 \mid \Delta_{JK} \mid 1 \rangle$ / kHz	0.2543(50)	$\langle 1 \mid q_{zJ} \mid 2 \rangle$ / kHz	-0.148(12)
$\langle 1 \mid \Delta_K \mid 1 \rangle$ / kHz	8.488(26)	$\langle 1 \mid q_{zK} \mid 2 \rangle$ / kHz	-0.660(89)
$\langle 1 \mid \delta_J \mid 1 \rangle$ / kHz	0.05655(46)	$\langle 1 \mid q_x \mid 2 \rangle$ / MHz	1.294(76)
$\langle 1 \mid \delta_K \mid 1 \rangle$ / kHz	1.399(17)	$\langle 1 \mid q_y \mid 2 \rangle$ / MHz	0.1508(57)
		$\langle 1 \mid h_v \mid 4 \rangle$ / MHz	-0.00952(26)
rms[b] / MHz	0.0014	N[c]	384
V_3 / cm^{-1}	411.59(46)	$\mid \lambda_z \mid$[e]	0.6972(35)
I_α / amu·Å^2	3.2055 [Fixed][d]	$\mid \lambda_x \mid$[e]	0.7075(52)
F / GHz	160.38	$\mid \lambda_y \mid$[e]	0.116(11)

[a] Values in parentheses denote 3 times standard deviation in units of the last digit.

[b] Root mean square deviation of the fit.

[c] Number of lines.

[d] Theoretical value obtained by ab initio calculation at MP2/aug-cc-pvtz.

[e] Absolute value of the direction cosine of the internal rotation axis to the molecular fixed *z*, *x* or *y* axis.

The analysis of the transition frequencies given in Table S-3 was carried out using a least-squares fitting procedure and spectroscopic parameters determined are given in Table 4. The root mean square deviation of the fit is 1.4 kHz, which is comparable to the measurement error of the transition frequency in our experiment. The barrier height V_3 and the direction cosine $|\lambda_z|$, $|\lambda_y|$ of the internal rotation parameters, which were estimated from $\langle 1 \mid q_g \mid 2 \rangle$ ($g = z, x, y$), $\langle 1 \mid A \mid 2 \rangle$, $\langle 1 \mid$

B | 2 ⟩, and ⟨ 1 | C | 2 ⟩ by using theoretical value of I_α and $\lambda_z^2 + \lambda_x^2 + \lambda_y^2 = 1$ restriction, are also given in Table 4. The experimental rotational constants and the direction cosines determined are similar to the theoretically calculated ones of both the In-a and In-b conformers of the insertion type complex of MG–H_2O (see ab initio results shown in Table 1). The magnitude of each component of the theoretical dipole moment indicates that In-a ($|\mu_a|$ = 2.36, $|\mu_b|$ = 1.00, $|\mu_c|$ = 0.25 D) is suitable rather than In-b ($|\mu_a|$ = 3.22, $|\mu_b|$ = 1.09, $|\mu_c|$ = 2.57 D) from a viewpoint of the observed relative intensities between *a*-, *b*- and *c*-type transitions mentioned above. Therefore, we concluded that the observed complex is the In-a conformer of MG–H_2O.

6. Discussion

6.1. Barrier height to the methyl group internal rotation V_3 of MG and MG–H_2O In-a

The barrier height to internal rotation V_3 of the ester methyl group of the In-a conformer of MG–H_2O is determined to be 411.6 ± 5 cm^{-1}, which is higher than that of MG (V_3 = 394.5 ± 1.0 cm^{-1}) by 17.1 cm^{-1}. Similar increase of the barrier height to the internal rotation of the ester methyl group was already observed in hydration complexes of methyl lactate (ML) by Thomas et al. [10]. ML is also an α-hydroxyester and is known to form insertion-type complexes with H_2O as well as MG. The internal rotation barrier height for the ML–H_2O i-I (most stable conformer among the monohydrates) and ML–$(H_2O)_2$ ii-II is 428 cm^{-1} and 434 cm^{-1}, respectively, higher than V_3 = 398 cm^{-1} of ML. Thomas et al. attributed the difference of V_3 to a decrease in the (C=)O⋯H(ester methyl) van der Waals distance(s) in ML after hydration. The (C=)O⋯H(ester methyl) distances in the optimized structure of the In-a conformer of MG–H_2O are shorter by about 0.02 Å in comparison with those of MG monomer, similarly to the case of ML–H_2O.

6.2. Conformational flexibility in the insertion complex of MG–H_2O

The barrier height to ring-inversion of the In-a conformer of MG–H_2O was estimated to be

306 cm^{-1}, from the observed vibrational energy difference $\Delta E_{10} = 2\langle 1 | h_v | 4 \rangle$ and theoretical structures of the In-a and "*Cs*"-conformation, by applying a simple approach described in Appendix A. The "*Cs*"-conformation (specified by "*Cs*" in Fig. 5 and Fig. 6) is expected to be the transition state of the ring-inversion between two equivalent forms of the In-a conformer. However, the theoretical energy difference between the "*Cs*"-conformation and the In-a equilibrium was calculated to be 915 cm^{-1} which is very large in comparison with the experimental barrier to ring-inversion.

In order to investigate the ring-inversion motion of MG–H_2O In-a in detail, we then performed a relaxed potential energy scan calculation as a function of the dihedral angle *D*(1-4-6-7), which specifies the orientation of H atom of the hydroxy group in MG subunit. At first, the scan was performed at intervals of 10 º from *D*(1-4-6-7) = 60.7 º of the In-a conformer to *D*(1-4-6-7) = −59.3 º. However, this relaxed potential energy scan did not provide the symmetric double minimum potential which corresponds to the large amplitude motion between two equivalent forms of the In-a conformer related by a mirror plane. The calculated potential curve is an unsymmetrical double minimum function associated with the isomerization between In-a " 1 " and In-b " 3 " as shown in Fig. 5-(a). Fig. 5-(a) also includes the results calculated at outer angle regions of the local minimums " 1 " and " 3 " as well as the results calculated near the local maximum " 2 " in detail. In the course of this isomerization path, the non-planar seven-membered ring of MG–H_2O (−C(1)=O(2)···H(14)−O(13)···H(7)−O(6)−C(4)−) inverts through a planar ring structure, but the free H(15) of water subunit is always located in the same side (above or below) with respect to a plane defined by O(2), O(6) and O(13) atoms. The local maximum " 2 " of this potential appears at *D*(1-4-6-7) ≅ −4 º, and the barrier heights from the In-a and In-b conformers were calculated to be 669 cm^{-1} and 467 cm^{-1}, respectively. Fig. 6 illustrates the structural change of MG–H_2O during the In-a ↔ In-b isomerization using the snapshots at the In-a equilibrium " 1 ", the local maximum " 2 ", and the In-b equilibrium " 3 ". In addition, dihedral angle dependence of the calculated rotational constants in this path is shown in Fig. 7-(a), using the rate of change from the In-a conformer

equilibrium.

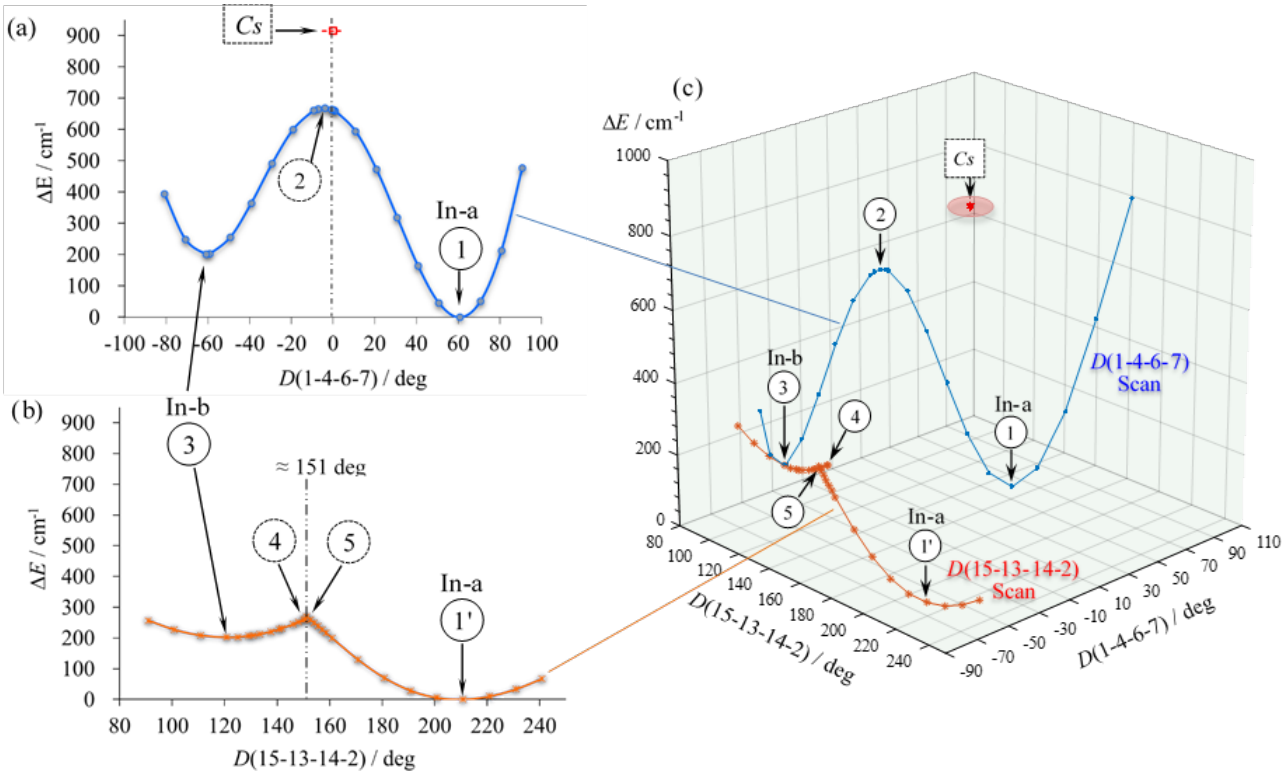

Fig. 5. The isomerization Potentials between the In-a and In-b conformers of MG–H_2O (MP2/aug-cc-pVTZ). (a) Result of *D*(1-4-6-7) scan which corresponds to the ring-inversion-type isomerization path. (b) Result of *D*(15-13-14-2) scan which corresponds to the torsional-type isomerization path. (c) Three dimensional potential curves of (a) and (b) along the *D*(1-4-6-7) and *D*(15-13-14-2) coordinates.

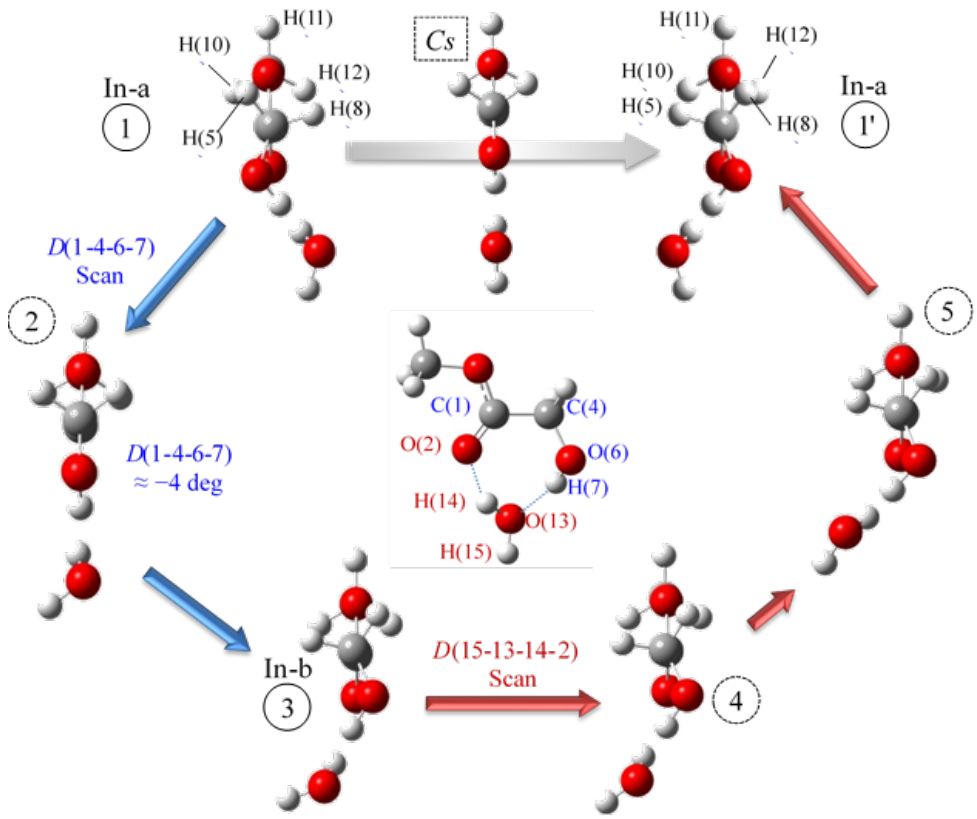

Fig. 6. Structural change of MG–H_2O during the In-a ↔ In-b isomerization illustrated by the snapshots at the key conformations assigned by " 1 " ~ " 5 ", " 1' " and "*Cs*" in Fig. 5. Definitions of the dihedral angles *D*(1-4-6-7) and *D*(15-13-14-2) are illustrated in a central image of the molecular structure.

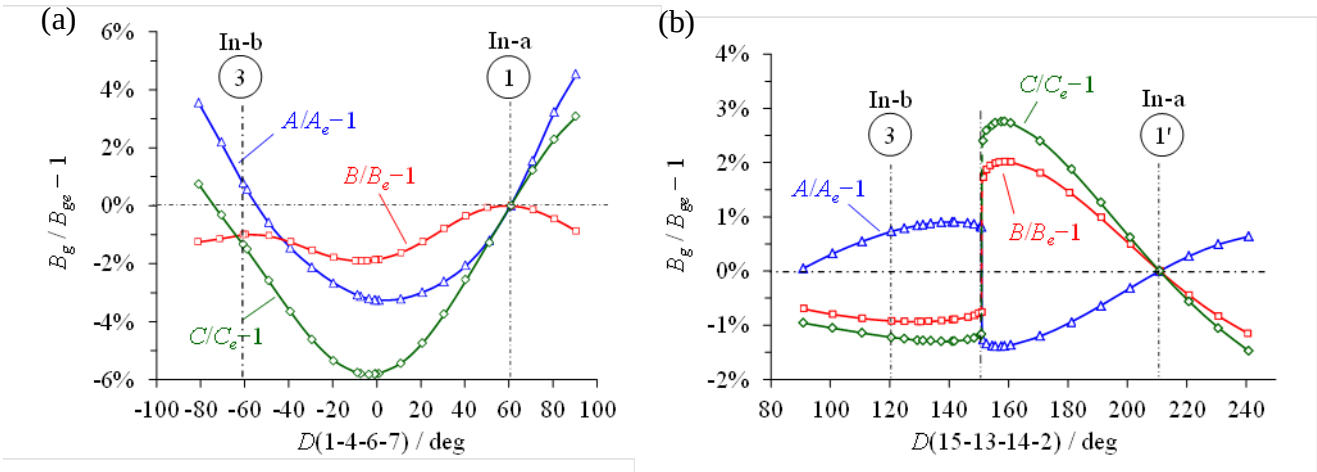

Fig. 7. Dihedral angle dependences of the calculated rotational constants (MP2/aug-cc-pVTZ) in the In-a ↔ In-b isomerization of MG-H_2O. (a) The ring-inversion-type isomerization path. (b) The torsional-type isomerization path.

Another different path for the In-a ↔ In-b isomerization was also examined by the relaxed potential energy scan as a function of the dihedral angle *D*(15-13-14-2). This isomerization path corresponds to the rotation of the free H(15) about the O(13)–H(14) bond in water subunit. The potential curve obtained and the snapshots of the structural change are illustrated in Fig. 5-(b) and Fig. 6, respectively, and the angle dependence of the rotational constants in the course of the isomerization path is shown in Fig.7-(b). As indicated particularly in Fig.7-(b), this isomerization path exhibits a discontinuity near *D*(15-13-14-2) = 151 º between "4" and "5". This potential consists of two kinds of shallow potential curves extended from In-a equilibrium and In-b equilibrium, and a curvilinear switching occurs at *D*(15-13-14-2) ~ 151 º. It is considered that an interchange of the lone pair which forms intermolecular hydrogen bond with MG occurs among two sets of the lone pair of H_2O at the discontinuity point. The discontinuity point is located in higher energy of 261 cm^{-1} relative to the In-a equilibrium and can be regarded as a local maximum of the isomerization potential. Evidently, this torsional-type path is more favorable than the former ring-inversion-type path for the In-a ↔ In-b isomerization. The conversion barrier from the In-b conformer to the In-a conformer was estimated to be very low of 59 cm^{-1}. According to the vibrational analysis for the In-b conformer carried out by the ab initio calculation, the harmonic vibrational frequency of a normal mode corresponding to this torsional isomerization path was calculated to be 207 cm^{-1}. The zero-point vibrational energy calculated from this value will exceed the conversion barrier. Therefore, we consider that In-b is not a stable conformer of MG–H_2O, and actually we could not detect it. Similar isomerization behavior of the ML–H_2O (i-I ↔ i-II isomerization) was discussed based on the ab-initio calculation by Thomas et al. [10]. On the other hand, for the In-a conformer, two normal modes which show similar torsional behavior of H_2O subunit were found. The harmonic frequencies of those are 242 and 261 cm^{-1}, accordingly it is expected that the vibrational ground state exists under the conversion barrier at least but performs the large amplitude vibration.

Fig. 5-(c) illustrates three-dimensional potential curves of the ring-inversion-type isomerization path and the torsional-type isomerization path along the *D*(1-4-6-7) and *D*(15-13-14-2) coordinates. It should be noted that the two equivalent positions (“ 1 ” and “ 1' ”) corresponding to the In-a conformer can be connected by a combination of these two isomerization paths. This combination path goes through lower barriers than that of the direct path which is linked through the *Cs*-symmetry conformation “ *Cs* “. It seems that the situation of the MG–H_2O complex with respect to the conformational landscape and flexibility is similar to that of the glycol aldehyde–H_2O complex reported by Aviles-Moreno et al. [24]. The two most stable conformers of these two complexes are the insertion-type complex having the same seven-membered intermolecular ring. However the barrier heights which should be exceeded in the ring-inversion motion are different among these two complexes as shown in Fig. 8. Only the most stable conformer is identified by the FTMW spectroscopy for both complexes. In the case of the glycol aldehyde–H_2O CC-W-1 complex, the *a*- and *b*-type transitions which exhibit ring-inversion doublet of small splitting width were observed, but the *c*-type transition which gives directly the information of the energy separation between two tunneling sublevels was not observed. Therefore, we are not able to discuss about the relation between the barrier heights and the ground state splitting width.

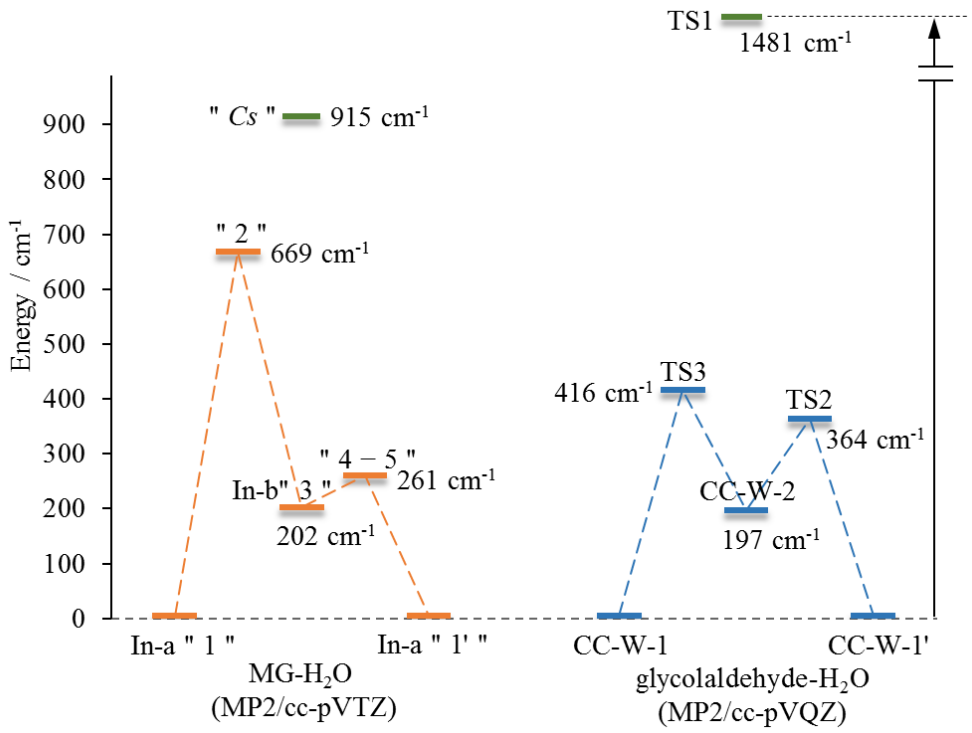

Fig. 8. Energy diagram corresponding to the isomerization and the ring-inversion motion of MG–H_2O (MP2/cc-pVTZ) and glycol aldehyde–H_2O (MP2/cc-pVQZ) [24].

It is interesting to note that the internal rotation of H_2O subunit about (C)O−H···O_W hydrogen bond was observed in the pyruvic acid–H_2O complex [25] which has similar hydrogen bond network of the seven-membered ring (−C=O···H_W−O_W···H−O−C−). This internal rotation exchanges the two H atoms of H_2O and causes the tunneling splitting with 3 : 1 intensity ratio to the rotational spectrum in accordance with nuclear spin statistics. On the other hand, the wagging motion of the free H atom of H_2O subunit through the *Cs* transition state, which corresponds to the ring-inversion motion in MG–H_2O and glycol aldehyde–H_2O, was concluded to be a barrier-less large amplitude vibrational motion which results in the planar structure effectively. We consider that this difference with respect to the conformational flexibility among these hydrates is mainly dependent on the torsional rigidity around the CC−OH bond of the monomer molecule. In the case of MG and glycol aldehyde, the torsion around the CC−OH bond of the monomer is hindered by a relatively low potential barrier and the intramolecular hydrogen bond stabilizes the planar ring structure of the

skeleton. Therefore, the torsional angle of the CC−OH bond changes by 40 º ~ 60 º from that of the monomer on forming the insertion complex. On the other hand, the CC−OH bond of pyruvic acid is more rigid due to its weak double bond character. Thus, the calculated torsional angle change in the pyruvic acid–H_2O complex is less than 2 º.

From the comparison of the theoretical results about the In-a and In-b conformers of MG–H_2O, it seems that the relation between the energy stability and the hydrogen bond length is inconsistent. As given in Fig. 5 and Table 1, In-b is unstable compared with In-a, although both of the lengths of two hydrogen bonds are shorter. Fig. 9 shows the scan coordinate dependences of Wiberg bond index for the two hydrogen bonds H(7)···O(13) and O(2)···H(14) and the deformation energy E_{def}(total) as a function of the dihedral angles D(1-4-6-7) and D(15-13-14-2) corresponding to the two kinds of paths of the In-a ↔ In-b isomerization, as well as the isomerization potential ΔE. At the equilibrium structure, since In-a and In-b have similar values of the hydrogen bond indexes and E_{def}(total), we cannot find the evident superiority of In-a. Wiberg bond indexes for O(2)···O(13) and O(6)···O(13) are also shown in Fig. 9. The value of O(6)···O(13) bond index for In-a is somewhat larger than that of In-b in comparison with other kinds of bond indexes.

Next, we consider change of the bond indexes and the deformation energy in the ring-inversion-type isomerization process shown in Fig. 9-(a). The H(7)···O(13) bond index curve has two local maximums in an inner area near the equilibriums of each conformer, and meanwhile, the two local maximums of the O(2)···H(14) bond index curve appear in an outer area near the equilibriums. Both curves have the local minimum near the local maximum of the potential energy, but the O(2)···H(14) bond index curve decreases more from its own local maximums in comparison with the H(7)···O(13) bond index. The magnitudes of the bond indexes suggest that the H(7)···O(13) hydrogen bond is stronger than the O(2)···H(14) hydrogen bond in the range of ~ - 75 º < D(1-4-6-7) < ~ 75 º. The deformation energy curve exhibits the shape of the shallow symmetrical valley centering on a potential maximum position and increases quickly in the outer area of the

equilibrium conformations. In the case of the torsional-type isomerization, dihedral angle dependences are small except for the H(7)···O(13) bond index, as shown in Fig. 9-(b). As mentioned above, the discontinuity near *D*(15-13-14-2) = 151 º originates from the lone pair interchange of H_2O in hydrogen bond formation. The remarkable discontinuity which appears in the H(7)···O(13) bond index indicates the evidence of the lone pair switching of the hydrogen bond.

These results indicate that the subtle balance between the hydrogen bond stabilization and the deformation energy caused by the hydrogen bond formation determines the conformation stability or conformational flexibility of the insertion complex of MG–H_2O. However, the strategy of examining Wiberg bond index and deformation energy cannot elucidate the final factor which determines the difference in the stability between the In-a and In-b conformers. We consider the dipole-dipole interaction between the MG and H_2O subunit of the complex as a possible candidate. The effect of this interaction is already taken into the electronic energy in the ab-initio calculation. Using the results of the virtual subunits MG and H_2O which were calculated in the deformation energy estimation, we computed the angle between the dipole moments of the subunits in MG–H_2O. The angle obtained for In-a is 120 º, accordingly, the dipole moments of two subunits are slightly opposite to each other, and it is expected that the dipole-dipole interaction reduces the energy. The angle in In-b is 46 º, the two dipoles have the similar orientation, and thus an energy increase is expected. In the case of In-a, in contrast to the magnitude of 2.57 D of theoretical dipole moment of the complex, the magnitude of the vector sum of the dipole moments of two subunits ($|\mu(MG)|$ = 2.56 D and $|\mu(H_2O)|$ = 1.97 D) is calculated to be 2.33 D. In the case of In-b, the magnitudes of the complex and the vector sum of the subunits ($|\mu(MG)|$ = 2.49 D and $|\mu(H_2O)|$ = 1.97 D) are 4.26 D and 4.11 D, respectively.

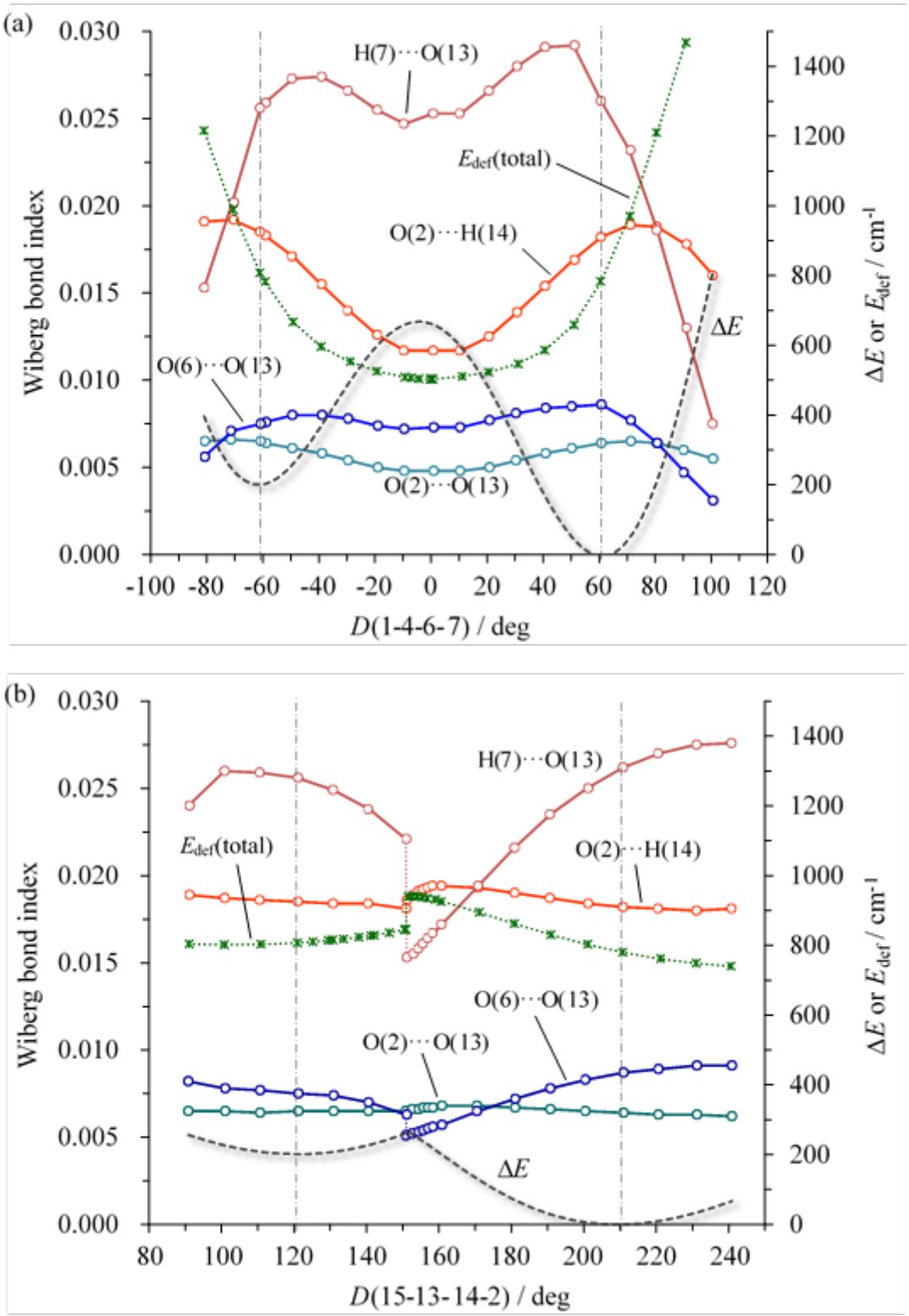

Fig. 9. The scan coordinate dependences of Wiberg bond index for the two hydrogen bonds H(7)···O(13) and O(2)···H(14) and the deformation energy E_{def}(total) as a function of the dihedral angles *D*(1-4-6-7) and *D*(15-13-14-2) corresponding to the two kinds of paths of the In-a ↔ In-b isomerization, as well as the isomerization potential Δ*E*. Wiberg bond indexes for O(2)···O(13) and O(6)···O(13) are also shown.

6. Conclusions

The rotational spectrum of one conformer of the methyl glycolate–H_2O (MG–H_2O) complex has been investigated using pulsed jet Fourier transform microwave spectroscopy. Among six most stable conformers of MG–H_2O optimized at the MP2/aug-cc-pVTZ level of theory, the observed conformer was assigned to the most stable In-a conformer of the insertion complex, in which the intramolecular hydrogen bond of MG monomer is ruptured and the intermolecular hydrogen bonds with H_2O form the non-planar seven-membered ring (−C=O···H_w−O_w···H−O−C−). The insertion complex of MG–H_2O has two possible conformers In-a and In-b, classified by the orientation of the hydrogen-bond free H atom in H_2O subunit. Furthermore, each conformer can take two equivalent structures interrelated by mirror-operation because of the high symmetry of MG. Observed spectrum exhibits splittings arising from the methyl internal rotation and the ring-inversion motion between two equivalent conformations, but the inversion splittings can be observed only in the c-type transition. Parameterized expressions of the Hamiltonian matrix elements suitable for the analysis of the rotational spectrum of the In-a (or In-b) conformer were derived by applying the tunneling matrix formalism developed by Hougen [11]. The barrier height to internal rotation of the methyl group V_3 and the direction cosine for the internal rotation axis were determined from the corresponding parameters determined. And it was found that the barrier height of In-a is higher than that of MG monomer by 17.1 cm^{-1}. For the ring-inversion motion, only the tunneling splitting of $2\langle 1 | h_v | 4 \rangle$ = 19 kHz between two sublevels was determined. Conformational flexibility, which corresponds to the large amplitude motion between two equivalent conformations and to the isomerization between the In-a and In-b two conformers of the insertion complex, was investigated with the help of the ab initio calculation. The ab initio calculation suggests that the combination of two different In-a ↔ In-b isomerization path provides more favorable low barrier pathway for the ring-inversion motion than the direct path which is linked through the “planar” conformation.

Appendix A. Estimation of the barrier to ring-inversion

We suppose that the inversion between two equivalent structures transforms the coordinates (x_i, y_i, z_i) of the i-th atom of the molecule into (x_i, y_i, $-z_i$), and that the transition state of the ring-inversion motion has planar symmetry (planar-ring structure). In order to treat the ring-inversion vibration as a one-dimensional motion, we assumed that the coordinates of each atom during the inversion motion can be written by the linear formula

$$g_i \cong g_{\mathrm{TS}i} + \beta_{gi} \times z_q \quad (g = x, y, z), \tag{A1}$$

where $g_{\mathrm{TS}i}$ indicates the coordinate in the transition state and z_q is the z-coordinate of the specific atom $i = q$ which is in the symmetry plane in the transition state. If the coefficients β_{gi} are the constants, we can evaluate them easily from the coordinates of atoms in the principal inertial axes system corresponding to the structures of equilibrium and the transient state by using

$$\beta_{gi} = \frac{g_{ei} - g_{\mathrm{TS}i}}{z_{eq}} \quad (g = x, y, z), \tag{A2}$$

where g_{ei} indicates the coordinate in equilibrium. The kinetic energy T for the inversion motion can be written approximately as

$$T = \sum_i \frac{1}{2} m_i \left[\left(\frac{dx_i}{dt} \right)^2 + \left(\frac{dy_i}{dt} \right)^2 + \left(\frac{dz_i}{dt} \right)^2 \right] = \frac{1}{2} M_{eff} \left(\frac{dz_q}{dt} \right)^2 , \tag{A3}$$

where m_i denotes the mass of each atom, and M_{eff} is an effective mass defined by

$$M_{eff} \equiv \sum_i m_i \left(\beta_{xi}{}^2 + \beta_{yi}{}^2 + \beta_{zi}{}^2 \right) . \tag{A4}$$

Thus, the magnitude of M_{eff} can be calculated by using optimized structures obtained by ab initio calculation. The following function was assumed as the potential energy:

$$V(z_q) = \begin{cases} V_{\mathrm{inv}} \left[1 - \left(\dfrac{z_q}{z_{eq}} \right)^2 \right]^2 & (-z_{eq} \le z_q \le z_{eq}), \quad \text{(A5-1)} \\ D\left[\exp\left(-2\alpha \left| z_q - z_{eq} \right|\right) - 2\exp\left(-\alpha \left| z_q - z_{eq} \right|\right) + 1 \right] & (\left| z_q \right| > z_{eq}), \quad \text{(A5-2)} \end{cases}$$

where

$$\alpha \equiv \frac{2}{z_{eq}}\sqrt{\frac{2V_{\mathrm{inv}}}{D}}\ . \tag{A6}$$

Here, z_{eq} is the absolute value of the equilibrium z-coordinate of the atom q, and V_{inv} is the barrier to inversion. In consideration of applying to the hydrogen bond complex such as MG–H_2O, we employed the Morse-type function [26] as given in Eq. (A5–2) for the range of $|\, z_q \,| > z_{eq}$. Furthermore, we introduced the relationship given by Eq. (A6) which makes the values of the second derivative of the functions given in Eq. (A5–1) and Eq. (A5–2) identical at the $z_q = z_{eq}$ limit. The vibrational energies and the eigen functions for the inversion motion were obtained by numerically solving the Schrodinger equation corresponding to the effective Hamiltonian with the form

$$H_{eff} = -\frac{\hbar^2}{2M_{eff}}\frac{\partial^2}{\partial z_q{}^2} + V\left(z_q\right). \tag{A7}$$

Although the magnitudes of M_{eff} and z_{eq} are deservedly dependent on choice of the atom q, the vibrational energies are not affected.

In this study, the barrier to inversion V_{inv} was estimated from the observed energy difference between the two lowest vibrational states ΔE_{10} and the theoretical M_{eff} value obtained by ab initio calculation at MP2/aug-cc-VTZ, using the Hamiltonian given in Eq. (A7). In order to examine the validity of this method, we applied it to the estimation of the barrier to ring-inversion (puckering) of cyclopentene, 1-chlorocyclopentene and Indan first. Sufficiently large value of 50000 cm^{-1} was presumed as the dissociation energy D for these monomers. The results are summarized in Table A1 and the estimated values of V_{inv} (underlined in the table) are compared with those which have already been determined by using conventional analyses [27 – 29]. It is confirmed that our method can provide the value of V_{inv} comparable to that reported in the previous study in the cases of these monomers. Theoretical values of V_{inv} which were evaluated in this study as the energy difference

between the equilibrium and the transition state are found to be 120 – 140 % of the experimental values, as shown in Table A1.

The barrier to inversion V_{inv} of MG–H_2O In-a was estimated to be 306 cm^{-1} from the observed value of $\Delta E_{10} = 2\langle 1 \mid h_v \mid 4 \rangle = 0.019$ MHz. The value of D was assumed to be 3000 cm^{-1} which is comparable with the dissociation energy of this complex. The result is also given in Table A1 with the theoretical V_{inv} which was calculated as the energy difference between the In-a equilibrium structure and the *Cs*-conformation (see Figs. 5, 6 and 8). Unlike the cases of cyclopentene, 1-chlorocyclopentene and Indan, the theoretical value of V_{inv} (915 cm^{-1}) is quite larger than the experimental value in the case of MG–H_2O. It should be noted here that the magnitude of D hardly affects the derived value of V_{inv} except for the case where it is very small. For example, we obtain V_{inv} = 309 cm^{-1} for MG–H_2O when D = 50000 cm^{-1} is assumed, and V_{inv} = 303 cm^{-1} when D = 1000 cm^{-1}.

Table A1

Parameters of the potential function defined by Eq. (A5) and observed vibrational energy differences ΔE_{01} of the ring-inversion motion of MG–H_2O In-a conformer and other selected molecules.

	MG–H_2O In-a	Cyclopentene	1-Chloro-cyclopentene	Indan
ΔE_{01} / MHz	0.0190(5)	27333.00(6)[a]	42328(10)[b]	22.364(1)[c]
V_{inv} / cm^{-1}	306[d] [915][e]	236(5)[a] 231[d] [290][e]	205(15)[b] 190[d] [254][e]	434[c] 461[d] [648][e]
D / cm^{-1}	3000	50000	50000	50000

[a] Ref. [27].
[b] Ref. [28].
[c] Ref. [29].
[d] Estimated in this work.
[e] Theoretical barrier obtained by ab initio calculation at MP2/aug-cc-VTZ.

Appendix B. Supplementary material

Supplementary data associated with this article can be found, in the online version, at _____.

References

[1] M. Brochu, P. Buckley, Can. J. Spectrosc. 18 (1973) 165 – 169.

[2] H. Hollenstein, R. W. Schär, N. Schwitzgebel, G. Grassi, H2. H. Günthard, Spectrochim. Acta. Part A 39 (1983) 193 – 213.

[3] W. Caminati, R. Cervellati, J. Mol. Struct. 81 (1982) 143 – 145.

[4] W. Caminati, R. Cervellati, Z. Smith, J. Mol. Struct. 97 (1983) 87 – 92.

[5] R. Meyer, W. Caminati, H. Hollenstein, J. Mol. Spectrosc. 137 (1989) 87 – 103.

[6] S. Jarmelo, R. Fausto, J. Mol. Struct. 509 (1999) 183 – 199.

[7] P. Ottaviani, B. Velino, W. Caminati, Chem. Phys. Lett. 428 (2006) 236 – 240.

[8] N. Borho, Y. Xu, Phys. Chem. Chem. Phys. 9 (2007) 1324 – 1328.

[9] J. Thomas, O. Sukhorukov, W. Jäger, Y. Xu, Angew. Chem. Int. Ed. 52 (2013) 4402 – 4405.

[10] J. Thomas, O. Sukhorukov, W. Jäger, Y. Xu, Angew. Chem. Int. Ed. 53 (2014) 1156 – 1159.

[11] J. T. Hougen, J. Mol. Spectrosc. 89 (1981) 296 – 327.

[12] M. Fujitake, J. Aoyama, N. Ohashi, J. Mol. Spectrosc. 235 (2006) 27 – 34.

[13] Gaussian 09, Revision C.01, M. J. Frisch, G. W. Trucks, H. B. Schlegel, G. E. Scuseria, M. A. Robb, J. R. Cheeseman, G. Scalmani, V. Barone, B. Mennucci, G. A. Petersson, H. Nakatsuji, M. Caricato, X. Li, H. P. Hratchian, A. F. Izmaylov, J. Bloino, G. Zheng, J. L. Sonnenberg, M. Hada, M. Ehara, K. Toyota, R. Fukuda, J. Hasegawa, M. Ishida, T. Nakajima, Y. Honda, O. Kitao, H. Nakai, T. Vreven, J. A. Montgomery, Jr., J. E. Peralta, F. Ogliaro, M. Bearpark, J. J. Heyd, E. Brothers, K. N. Kudin, V. N. Staroverov, T. Keith, R. Kobayashi, J. Normand, K. Raghavachari, A.

Rendell, J. C. Burant, S. S. Iyengar, J. Tomasi, M. Cossi, N. Rega, J. M. Millam, M. Klene, J. E. Knox, J. B. Cross, V. Bakken, C. Adamo, J. Jaramillo, R. Gomperts, R. E. Stratmann, O. Yazyev, A. J. Austin, R. Cammi, C. Pomelli, J. W. Ochterski, R. L. Martin, K. Morokuma, V. G. Zakrzewski, G. A. Voth, P. Salvador, J. J. Dannenberg, S. Dapprich, A. D. Daniels, O. Farkas, J. B. Foresman, J. V. Ortiz, J. Cioslowski, D. J. Fox, Gaussian, Inc., Wallingford CT, 2010.

[14] S. F. Boys, F. Bernardi, Mol. Phys. 19 (1970) 553 – 566.

[15] S. Simon, M. Duran, J. J. Dannenberg, J. Chem. Phys., 105 (1996) 11024-11031.

[16] K. B. Wiberg, Tetrahedron 24 (1968) 1083 – 1096.

[17] N. Ohashi, J. T. Hougen, to appear in J. Mol. Spectrosc (2017).

[18] P.-O. Löwdin, J. Chem. Phys. 18 (1950) 365 – 375.

[19] J. K. G. Watson, in: J. R. During (Ed.), Vibrational Spectra and Structure, Vol. 6, Elsevier, New York, 1977.

[20] W. Gordy, R. L. Cook, “Microwave Molecular Spectra”, John Wiley & Sons, Inc., New York, 1984,

[21] J. D. Swalen, D. R. Herschbach, J. Chem. Phys. 27 (1957) 100 – 108.

[22] C. C. Lin, J. D. Swalen, Rev. Mod. Phys. 31 (1959) 841 – 892.

[23] D. R. Hershbach, J. D. Swalen, J. Chem. Phys. 29, (1958) 761 – 776.

[24] J.-R Aviles-Moreno, J. Demaison, T. R. Huet, J. Am. Chem. Soc. 128 (2006) 10467 – 10473.

[25] E. G. Schnizler, N. A. Seifert, S. Ghosh, J. Thomas, Y. Xu, W. Jäger, Phys. Chem. Chem. Phys. 19 (2017) 4440 – 4446.

[26] P. M. Morse, Phys. Rev. 34, 57–64 (1929).

[27] Juan C. López, Jose L. Alonso, M. Elena Charro, Georges Wlodarczak, and Jean Demaison, Journal of Molecular Spectroscopy 155, 143-157 (1992).

[28] Walther Caminati, Roberto Danieli, Adolfo C. Fantoni, and Juan C. López, Journal of Molecular

Spectroscopy 181, 91-98 (1997).

[29] Laura B. Favero, Weixing Li, Giancarlo Spadini, and Walther Caminati, Journal of Molecular Spectroscopy 316, 45-48 (2015).

Figure captions:

Fig. 1. Optimized geometries of the MG monomer and the six most stable conformers of the MG–H_2O complex calculated at the MP2/aug-cc-pVTZ level of theory. The relative energies and the hydrogen bond length are also given for the MG–H_2O complexes.

Fig. 2. Examples of the representative spectrum of MG–H_2O. (a) and (b) are the *a*- and *b*-type transitions, respectively, and exhibit the methyl group internal rotation doublet structure. (c) is the *c*-type transition which shows a quartet structure caused by the internal rotation and the ring-inversion motion.

Fig. 3. Intensity anomalies observed in the *b*- and *c*-type transition group of $(J, K_a) = (3, 3) – (2, 2)$ of MG–H_2O.

Fig. 4. Symmetrical triplets observed in the E-symmetry species of the *c*-type transitions, $5_{3\,3} – 4_{2\,3}$ and $5_{3\,2} – 4_{2\,2}$, of MG–H_2O.

Fig. 5. The isomerization potentials between the In-a and In-b conformers of MG–H_2O (MP2/aug-cc-pVTZ). (a) Result of *D*(1-4-6-7) scan which corresponds to the ring-inversion-type isomerization path. (b) Result of *D*(15-13-14-2) scan which corresponds to the torsional-type isomerization path. (c) Three dimensional potential curves of (a) and (b) along the *D*(1-4-6-7) and *D*(15-13-14-2) coordinates.

Fig. 6. Structural change of MG–H_2O during the In-a ↔ In-b isomerization illustrated by the snapshots at the key conformations assigned by " 1 " ~ " 5 ", " 1' " and "*Cs*" in Fig. 5. Definitions of the dihedral angles *D*(1-4-6-7) and *D*(15-13-14-2) are illustrated in a central image of the molecular structure.

Fig. 7. Dihedral angle dependences of the calculated rotational constants (MP2/aug-cc-pVTZ) in the In-a ↔ In-b isomerization of MG-H_2O. (a) The ring-inversion-type isomerization path. (b) The torsional-type isomerization path.

Fig. 8. Energy diagram corresponding to the isomerization and the ring-inversion motion of MG–H_2O (MP2/cc-pVTZ) and glycol aldehyde–H_2O (MP2/cc-pVQZ) [24].

Fig. 9. The scan coordinate dependences of Wiberg bond index for the two hydrogen bonds H(7)···O(13) and O(2)···H(14) and the deformation energy E_{def}(total) as a function of the dihedral angles *D*(1-4-6-7) and *D*(15-13-14-2) corresponding the two kinds of paths of the In-a ↔ In-b isomerization, as well as the isomerization potential ΔE. Wiberg bond indexes for O(2)···O(13) and O(6)···O(13) are also shown.